THE UNIVERSITY OF MANITOBA

MAGNETIC HARDENING IN $FePt_{1-x}Ni_x$ ALLOYS

by

G. HADJIPANAYIS

A THESIS

SUBMITTED TO THE FACULTY OF GRADUATE STUDIES

IN PARTIAL FULFILMENT OF THE REQUIREMENTS FOR THE DEGREE

OF MASTER OF SCIENCE

DEPARTMENT OF PHYSICS

WINNIPEG, MANITOBA

May, 1974

ACKNOWLEDGMENTS

I am indebted to Dr. P. Gaunt, who supervised the research project, for his interesting and helpful discussions. His encouragement throughout the course is greatly appreciated.

Thanks are also due to Mrs. Janice Pritchard for the excellent job she has done in typing the manuscript.

ABSTRACT

Several ternary alloys of the type $FePt_{1-x}Ni_x$ have been made from the FePt system, by replacing some Pt atoms with Ni atoms. The densities and the lattice parameters of these alloys were measured. After various heat treatments, the magnetization, the coercive force and the remanence were investigated. Measurements of the temperature dependence of the coercivity and remanence were made. An attempt was made to estimate roughly the magnetocrystalline anisotropy as well as the domain wall energy. Possible permanent magnetic properties were discussed. The results are summarized as follows.

a. All the alloys up to 30% Ni form the continuous solid solution and by suitable heat treatment they undergo the transformation from the disordered cubic structure to the ordered face-centered tetragonal of the AuCu type. This transformation produces a high magnetic hardness.

b. In the alloys containing more than 30% Ni, no useful permanent magnetic properties were observed, because of the presence of the ordered cubic compound Fe_3Pt.

It is suggested that the magnetic hardening is associated with small misoriented tetragonal regions, which act as pinning sites to the domain wall motion.

TABLE OF CONTENTS

LIST OF FIGURES

LIST OF TABLES

CHAPTER 1

THEORETICAL CONCEPTS

1.1 Introductory Remarks

A large number of materials may be grouped under the heading of ferromagnetics since, in certain respects, all are similar and they are quite distinctly characterized by their magnetic properties. Below a certain critical temperature, called the Curie temperature, a ferromagnetic becomes spontaneously magnetized, the value of magnetization increasing with decreasing temperature rapidly at first, and then slowly rising to a maximum at absolute zero (Figure 1.1).

Ferromagnets are further characterized by the phenomenon of hysteresis. Figure 1.2 shows how the magnetization M varies in a typical specimen when an external field H is applied; when the field is removed, the specimen retains some of its magnetization M_R, and extra energy supplied by the reverse field Hc is required to reduce the magnetization to zero. MR, the magnetization retained by a specimen in zero field under such conditions is termed its remanence or remanent magnetization and the reverse field H_C necessary to reduce the magnetization from its remanence intensity to zero, is

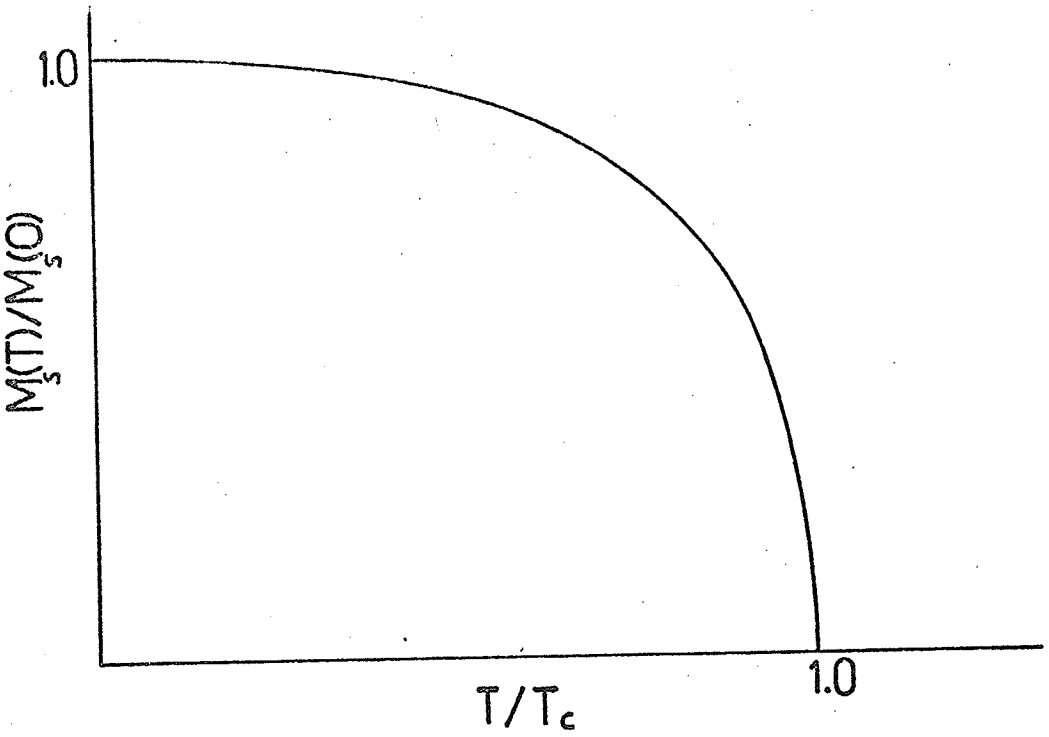

Fig.1.1. Variation of Spontaneous Magnetization with Temperature.

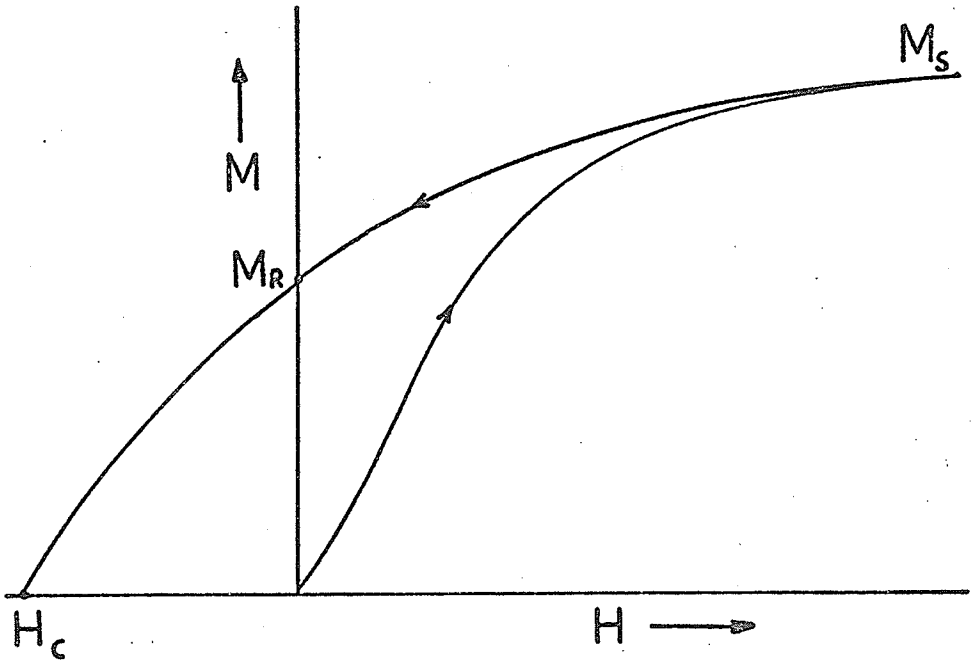

Fig. 1.2. The Magnetization M as a Function of the Applied Field H.

known as the coercive force or coercivity. There is also another term usually used in the literature which is called remanent coercivity H_R. This is defined as the field required to reduce the remanent magnetization to zero.

To account for the very high intensity of magnetization which a ferromagnetic crystal may acquire at ordinary temperatures and in relatively low magnetic fields, Weiss[1] (1907) postulated the presence of a large, internal molecular field, proportional to the magnetization. However, in practice and as may be seen from the experimental curve of Fig. 1.2 ferromagnetic crystal can exist in a state of zero overall magnetization. The fact led Weiss to suggest further that such crystals are magnetically saturated in small regions (domains) which are randomly oriented, so that in the demagnetized state the resultant magnetization of the crystal along any direction is zero. According to this the effect of an applied field is not to induce the magnetization at the atomic level, but to align the magnetization vectors of these domains.

1.2 Origin of Domains

Generally the main reason for the existence of domains in a crystal is that their formation reduces the magnetic free energy associated with it. The adopted procedure has been to postulate a domain

configuration for the demagnetized state complying with zero divergence of the magnetization. Then the dimensions of the domains can be calculated by minimizing the total free energy Wt, which may have the form,

$$Wt = Wex + Wk + Wm + W6 + Wo$$

on the basis of the chosen configuration.[2] Wex is the exchange energy due to the exchange interaction, Wk is the crystalline anisotropy energy which comes from the fact that it is easier to magnetize the crystal in certain directions ("easy directions") than in others. Wm is the magnetostatic energy, the energy of the crystal's magnetization in an applied field plus its energy in its own field. $W\sigma$ is the magnetostrictive energy associated with the fact that a ferromagnet exhibits changes in volume when placed in a magnetic field. Wo any other present form of energy.

Brown[3] (1962) also studied the minimization of the free energy without postulating a domain configuration. According to this, the basic concept is a spontaneous magnetization whose direction varies continuously with position in the lattice.

1.3 Domain Walls - Domain Wall Energy

From previous section we have seen the necessity of randomly oriented domains in a ferromagnetic crystal. The term "domain wall" denotes the transition layer which separates adjacent domains magnetized in different

directions. The nature of this boundary between domains is not an abrupt change of magnetization but rather a gradual one, since the latter involves less exchange energy. Within the wall the tendency of the exchange interaction to make the spins parallel is overcome and each spin is misaligned slightly from its neighbours, the wall width being usually determined by a competition between the exchange energy and the crystalline anisotropy. Calculations[4] have been done on this basis for an uniaxial specimen giving for the wall energy

$$\gamma = \alpha\pi (2E|k|)^{\frac{1}{2}} \quad \text{and for the wall width}$$

$$\delta = \alpha\pi \left(\frac{E}{2|k|}\right)^{\frac{1}{2}}$$

where E is the exchange energy, k is the anisotropy constant and α the interatomic distance.

1.4 Irreversible Process - Motion of Walls

Under the action of an applied magnetic field, the resultant magnetic moment of the specimen is increased in value. This could be visualized as taking place on the domain theory by two independent processes: by an increase in the volume of domains which are favorably oriented with respect to the field at the expense of unfavorably oriented domains or by rotation of the direction of magnetization towards the direction of the field.

On closer examination it comes out that in weak fields the magnetization changes usually proceed

by means of domain boundary displacements and in strong fields the magnetization usually changes by means of rotation of the direction of magnetization (Figure 1.3).

If all the processes taking place during a change in the magnetization of a crystal were reversible then the coercivity would be zero, and the existence in practice, of a finite coercivity suggests that the crystal is to some extent imperfect. The total energy of the specimen depends on the location of the wall because of this imperfection. For example, Figure 1.4 represents diagramatically the variation of the wall energy γ of a single 180° wall with its positions as measured along x axis. When the field is zero the wall will be at an energy minimum state. By applying a small field H the wall will move to a position where the driving force is balanced by the restoring force. The equilibrium position at A is determined by

$$2HM_s = \left(\frac{d\gamma}{dx}\right)_A$$

The action of the increasing field is to displace the wall to the right until it arrives to a position at B where $\frac{d\gamma}{dx}$ is maximum and

$$2HM_s = \left(\frac{d\gamma}{dx}\right)_{max.}$$

A further increase in the field causes the wall to move spontaneously and irreversibly to position C where

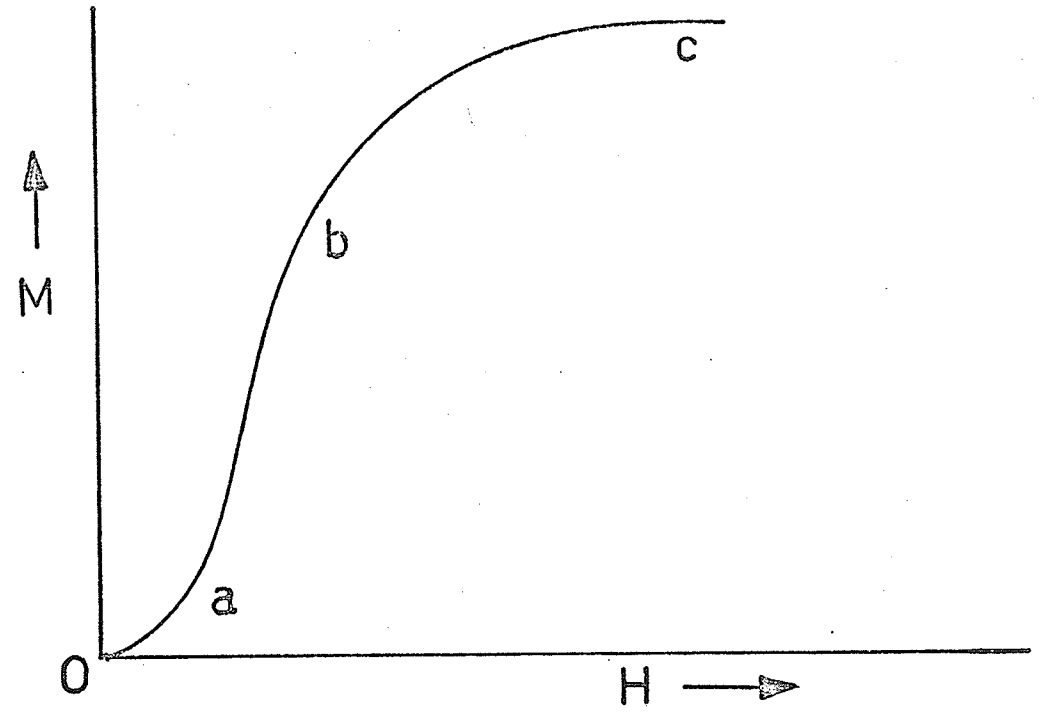

Fig. 1.3. Magnetization curve, showing the dominant magnetization processes in different regions of the curve. Oa reversible boundary displacement, ab irreversible boundary displacements, bc magnetization rotation.

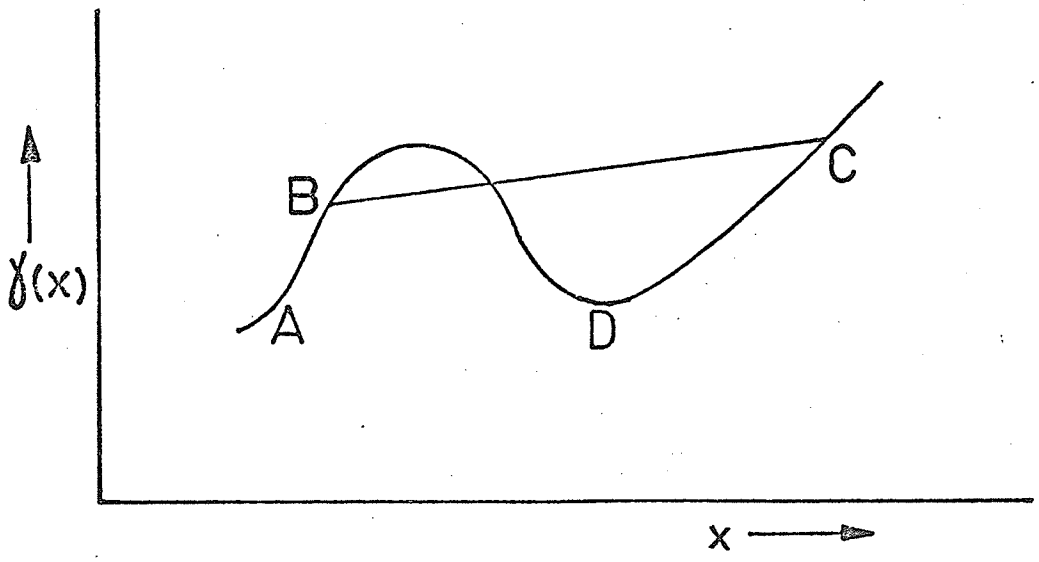

Fig. 1.4. Schematic variation of 180^{o} wall energy $\gamma(x)$ with position x

$$\left(\frac{d\gamma}{dx}\right)_C = 2HMs$$

the irreversible process causes a loss of energy and this is one of the factors giving rise to hysteresis.

1.5 Theories of Coercivity

The coercivity is a measure of the applied field required to move a wall over the energy barriers, and depends on the maximum slope of the domain wall energy. So in order to calculate this quantity, it is necessary to have an expression for the wall energy . For this, two things are required: first the kind of the imperfections and their contribution to the energy and secondly the distribution of the imperfections throughout the material. Consequently, many of the theories put forward to account for the coercivity have been concerned with mechanisms that might produce a variation of domain wall energy with position.

1.5.1 According to the strain theory[5] (1938, Becker) which is the first one developed, the existence of inhomogeneous stresses within a crystal might be a dominant factor in determining the resistance to domain wall motion. The local internal stresses lead to local variation of the magnetostrictive energy plus the domain wall energy. These internal stresses which are present in a ferromagnetic material can be affected by a convenient metalurgical process, such as cold working

plastic deformation or heat treatment. The maximum coercivity calculated by this model could be about 100 Oe.

1.5.2 The inclusion theory[6] (1943, Kersten) considers variations of domain wall energy caused by the intersection of the wall by a number of nonferromagnetic inclusions presented within the crystal. Coercivities obtained by this model are between the range of 1 - 10 Oe.

1.5.3 In the disperse field theory[7] (1944, 1946) Neel pointed out that the magnetic energy associated with inclusions or strain variations could be considerably greater than the changes of the wall energy associated with the same structure. This magnetostatic energy could be reduced by the formation of subsidiary domains based on the inclusions these domains are called "Neel spikes." Taking that into account, Neel calculated the coercive force which seems to account for values over 100 Oe.

1.5.4 The fine particle theory[8] is dealing with the existence of single domain particles whose size is so small, that below a critical value domain walls will not form, and the most stable state is the uniformly magnetized one. The irreversible process takes place by means of the rotation of the magnetization of the single domain. Several kinds of anisotropy, such as shape, crystalline and strain anisotropy could be taken

into account and for each one the coercivity is calculated by balancing the torques exerted on the magnetization vector of the single domain. These torques are due to the external applied field and to the considered anisotropy. This model is of great importance because of the high values of coercivity which can be obtained. The maximum theoretical values are of the order of $2\pi M_s$, $\frac{2k}{M_s}$ or $\frac{3\lambda_s 6}{M_s}$ for shape, crystalline and strain anisotropy, where 6 is the strain and λ_s the magnetostriction coefficient. For iron the maximum coercivity due to shape anisotropy could be 10,700 Oe.

1.5.5 The theories discussed so far, except Fine particle theory, have all been concerned with impedances to domain wall motion and they can apply to low coercivity materials rather than permanent magnets. Also, the fine particle theory which is widely applicable to many magnetically hard materials is inadequate to explain the behaviour of a group of permanent magnets like PtCo and $SmCo_5$.

P. Gaunt[9] trying to explain the magnetic properties of PtCo suggested a simple model of domain wall pinning by inhomogenetics in ferromagnetic alloys. Assume a 180^o domain wall which lies parallel to y, z plane and moves towards the x direction after the application of a field. Its wall energy can vary with

position as shown in Figures 1.5, 1.6. When a field is applied, an area A of the wall is displaced by a distance x so that the total magnetic energy can be written

(1) $U = A\gamma(x) - 2HMAx$

where $\gamma(x)$ is the wall energy per unit area and M is the saturation magnetization per unit volume. By minimizing this magnetic energy we can find the maximum or minimum stationary states. From previous sections we have seen that the coercive force is the field required to push a wall over the barrier. At absolute zero, this is given by $\frac{d^2U}{dx^2} = 0$, $\frac{dU}{dx} = 0$ and has the value of

(2) $$Ho = \frac{1}{2M}\left(\frac{d\gamma}{dx}\right)_{max.}$$

In fact in a pure phase there is a random distribution of these inhomogeneties whose area is less than the area A of the domain wall. Consequently at a finite temperature T most of the pinned area will vibrate due to thermal fluctuation effects. At this temperature, the coercive force will be less than Ho. Equation (1) can be rearranged so that it gives us the energy barrier

$$\Delta U = U_{max.} - U_{min.} = A\left[\gamma(x_2) - \gamma(x_1)\right] - 2HMA\,(x_2 - x_1)$$

where x_1, x_2 refers to the minimum and maximum energy.

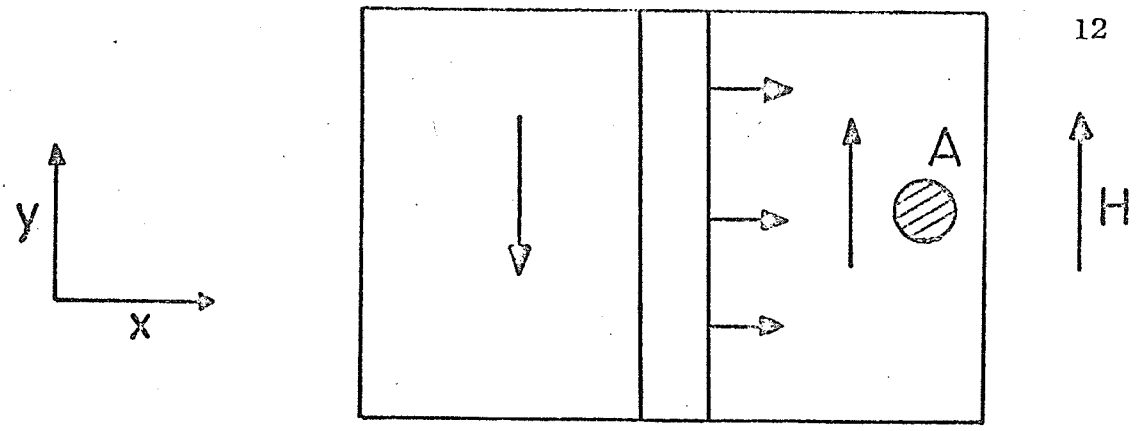

Fig. 1.5. 180^{o} domain wall approaching magnetically inhomogenous region.

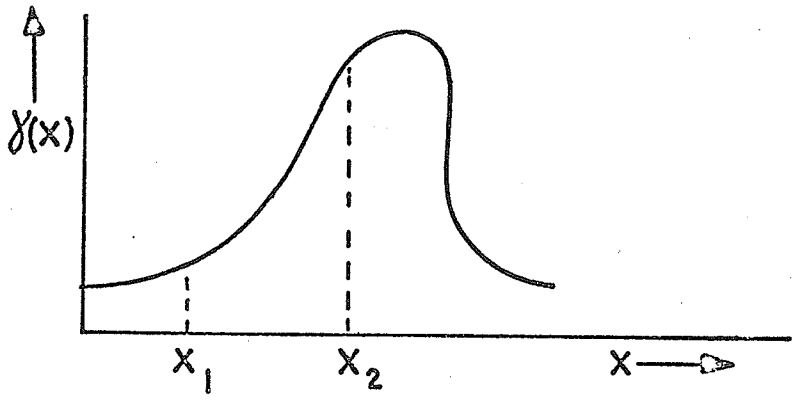

Fig. 1.6. Variation of wall energy with distance X travelled by the domain wall through the specimen shown in Fig. 1.5.

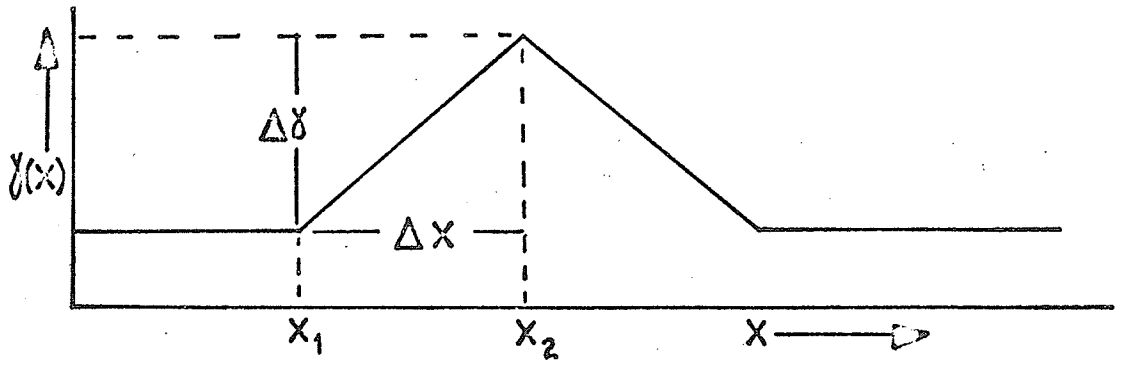

Fig. 1.7. Idealised wall energy variation with position "delta form."

Thermal activation energy will supply the wall with the energy needed to cross the barrier. The probability that the wall will pass the barrier in time τ is given by

(3) $$\frac{1}{\tau} = C \exp\left(-\frac{\Delta U}{kT}\right) \text{ where } C = 10^{12} \text{ sec}^{-1}$$

and τ can be arbitarily chosen as 1 sec., the time needed to make a measurement. Taking the logarithm of equation (3) we get

(4) $$0 = 25 - \frac{\Delta U}{kT}$$ and substituting the value of ΔU

(5) $$Hc = \frac{\Delta\gamma}{2M\Delta x} - \frac{25kT}{2MA\Delta x} \quad \text{or}$$

(6) $$Hc = Ho - \frac{25kT}{2MA\Delta x} \quad \text{where}$$

$$Ho = \frac{\Delta\gamma}{2M\Delta x}$$

From this equation it is obvious that Hc is always less than Ho, and that it is calculated if the form of $\gamma(x)$ is known. The "delta form" of the variation of the domain wall energy with position (Figure 1.7), is the simplest one we can consider, and it leads to the linear dependence of coercivity with temperature. Considering Figure 1.7 we can easily see that $2\Delta x$ is the width of inhomogenity and $A\Delta\gamma$ is the increase in wall energy associated with it.

Differentiating equation (6) with respect to T we may find

(8) $$\frac{dHc}{dT} = \frac{25k}{2MA\Delta_x}$$

and dividing equations 7, 8

(9) $$\frac{Ho}{\left(\frac{dHc}{dT}\right)} = \frac{A\Delta\gamma}{25k}$$ from which

we may find the change in the domain wall energy associated with an inhomogenity.

According to this model, for high coercivities a large and abrupt change of the domain wall energy with position is required.

1.6 Permanent Magnets

On the basis of the theories we have seen before, we can classify the magnetic materials as hard or soft according to their intrinsic coercive force. The range of variation of coercive force may be between 0.001 (supermalloy)--30,000 oe such as $SmCo_5$. Usually hard magnetic material may be defined as a substance with high coercive force, say above 100 oe.

In order for a material to serve as permanent magnet two things are necessary: a large value of remanence and a high coercivity. Analyzing the performance of permanent magnets it is essential to consider B versus H where B is the magnetic induction. The maximum energy product BH obtained on the demagnetizing branch, has become a standard, characterizing the quality of a permanent magnet material. The maximum

obtained value of this product[10] is $(BH)_{max.}$ = $9.6\ 10^6$ (Gauss x Oe) for CoPt.

CHAPTER 2

PREVIOUS AND PRESENT WORK ON FePt SYSTEMS

2.1 Previous Work on FePt Systems

The magnetic properties of iron-platinum alloys were first investigated by Graf and Kussman[11] (1935). They examined the magnetic hardness of these alloys and they attained a maximum coercivity of 1,800 Oe for the equatomic alloy quenched from the single phase at 1,200° C. The remanence induction was 3,500 gauss and (BH) max. = 3.1×10^6 (gauss.Oe). Lipson[12] followed a different procedure. He heated the alloy for a short time at 1,500°C and then he quenched it in air finding for Hc = 1,200 Oe. X-ray work showed that the alloy was an ordered f.c.t. structure with c = .968. The high coercivity was ascribed to strains introduced by the transformation from the high temperature cubic to the tetragonal phase.

Later Kussman and V. Ritteberg[13] found that for an at 40% Pt the saturation and remanence magnetization are higher while the coercive force is almost the same. They also found that the magnetostriction coefficient is very low so that the magnetic hardness is not due to the strain but to the high magnetocrystalline energy

of the tetragonal phase.

In contrast with the bulk material Weil[14] showed that the powders of ordered Fe-Pt phase has a very high coercivity up to 20,000 Oe (by extrapolation).

Recently V. Vlasova and Y. E. Vintaykin[15,16] have done a lot of work in these alloys. They studied the fine structure of FePt and they investigated the influence of plastic deformation and tempering on the coercive force, obtaining coercivities up to 7,400 Oe with $(BH)_{max.} = 7.6 10^6$ (gauss.Oe).

On the other hand Shotaro Shimize and Eigo Hashimoto[17] prepared the quasi binary alloys $Pt_{50-x}Pd_x Fe_{50}$ and $Pt_{50}Fe_{50-x}Ni_x$ and they examined their magnetic properties. They found that the alloys containing more than 20 at. % Pd are good from the viewpoint of permanent magnets, while those having more than 30% at. Ni they are not suitable as permanent magnets because they have low saturation magnetization and their magnetic transition temperature falls near to room temperature.

According to the phase diagram[18] (Fig. 2.1) in Fe-rich FePt alloys two types of ordered structures are formed with stoichiometric compositions Fe_3Pt and FePt, the first of which is analogous to Cu_3Au and the other to CuAu. The ordered FePt exists in the range of 30 - 65% at Pt and has a tetragonal structure. Fe and Pt atoms are disposed in layers parallel to $\{100\}$ planes. Around

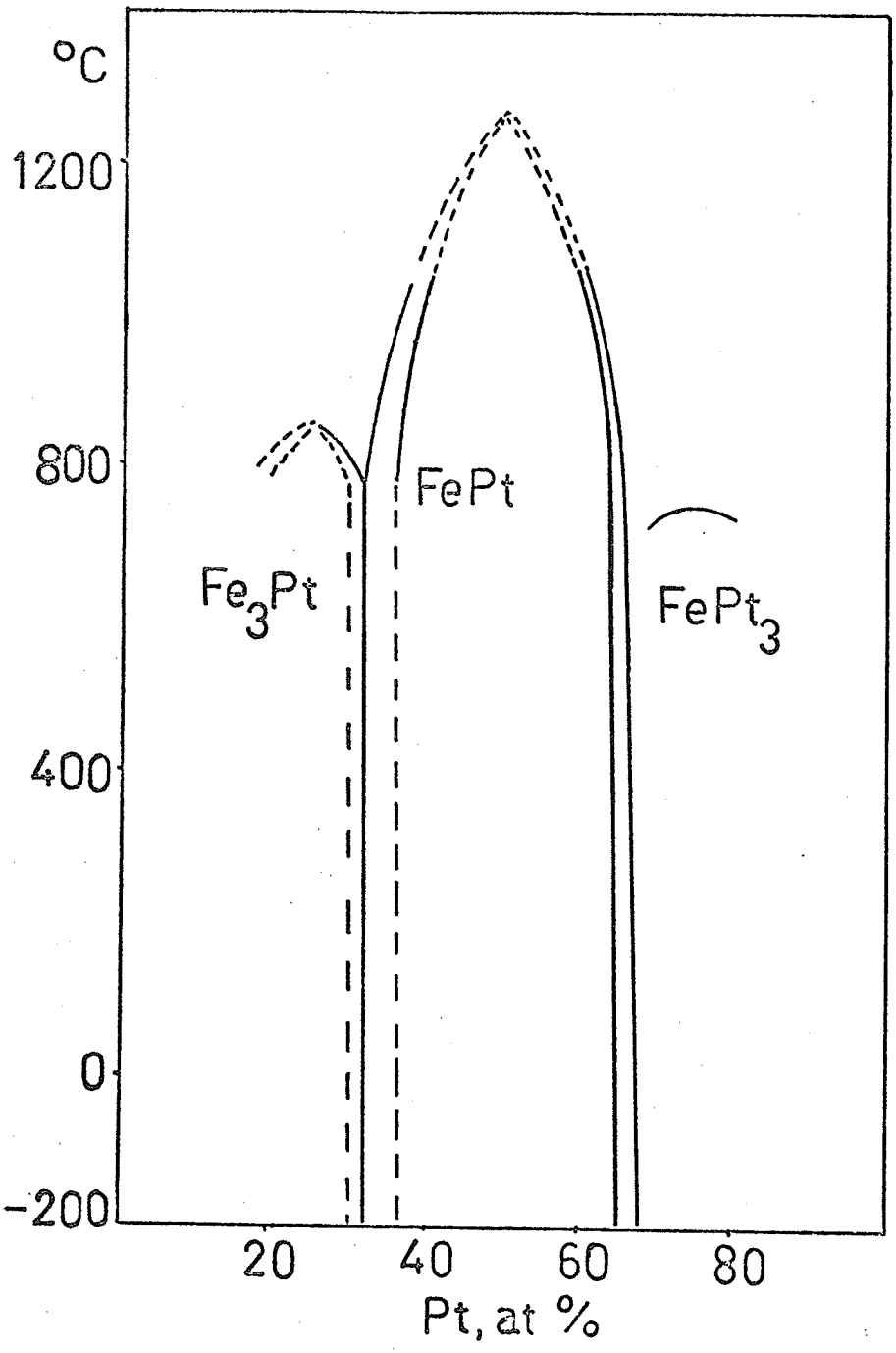

Fig. 2.1. Phase diagram of FePt.

the stoichiometric composition there are two narrow phase regions which show that the formation of the FePt superstructure is a first order transition.

2.2 Purpose of Present Work

It has been shown[19,20] recently that an Fe-Ni alloy at its equiatomic composition could exist in the ordered structure of AuCu type. Looking at this information, it was thought that a system with higher saturation magnetization, based on FePt, could be developed by substituting partially some of the Pt with Ni.

Apparently from the behavior of the new system, it is found that Ni takes the place of Fe atoms and this puts a limit in the amount of Ni for which ordered structure of the type AuCu could exist in the specimen (Fig. 2.1).

CHAPTER 3

EXPERIMENTAL PROCEDURE

3.1 Preparation of Samples

The ternary $FePt_{1-x}Nx$ alloys were melted by arc casting from high purity materials in a water cooled copper boat under an atmosphere of purified argon. For a high homogeneity , the alloys were remelted six times. The maximum weight losses from melting were .5% due to the splattering of Fe and Pt because they were in the form of thin wires.

After the alloys were produced, samples were cut off using the diamond wheel, and a final shape approximate to a prolate ellipsoid was obtained. Then the samples were entered in a solution of Nitric acid 45% and HCl 15% and they were ready for the heat treatment.

These samples were sealed into a clean vycor tube under 180 mm Hg pressure of Argon and they were homogenized at $1050^{o}C$ for several hours. From this high temperature the specimen were quenched by breaking the vycor tube under tap water.

Furthermore the specimen were subjected to a cumulative ageing process at various fixed temperatures, each time being quenched in the above way.

All the annealing was done in tube furnaces with temperature control of $\pm 2^{o}C$.

3.2 Apparatus

The ballistic method was used for the magnetization measurements. The maximum available magnetic field $\pm$ 16KOe, was provided by a water cooled electromagnet.

By withdrawing the sample from the uniform field region of the magnet, a voltage proportional to the magnetic moment of the sample is induced due to the change in flux in a 15,000 turns pick up coil. This voltage is fed into an electronic integrator (Fig. 3.1) based on a chopper stabilized operational amplifier. The output is displayed on a digital voltmeter.

Magnetic measurements at low temperatures up to $95^{o}K$ were obtained by using a cold finger arrangement (Fig. 3.2). The sample was mounted on one end of a copper rod, and the other end was cooled to LiN_2. A heater was sitting inside this end to fix the desired temperature and the copper rod was thermally isolated from the environment by a vacuum jacket. Using this method, equilibrium temperatures could easily be reached within $\pm 1^{o}K$.

A different set up was used for reaching $77^{o}K$. The sample was mounted on a vycor tubing which was fitted inside the magnet bore. Then by flushing LiN_2 through that tubing $77^{o}K$ could easily be reached.

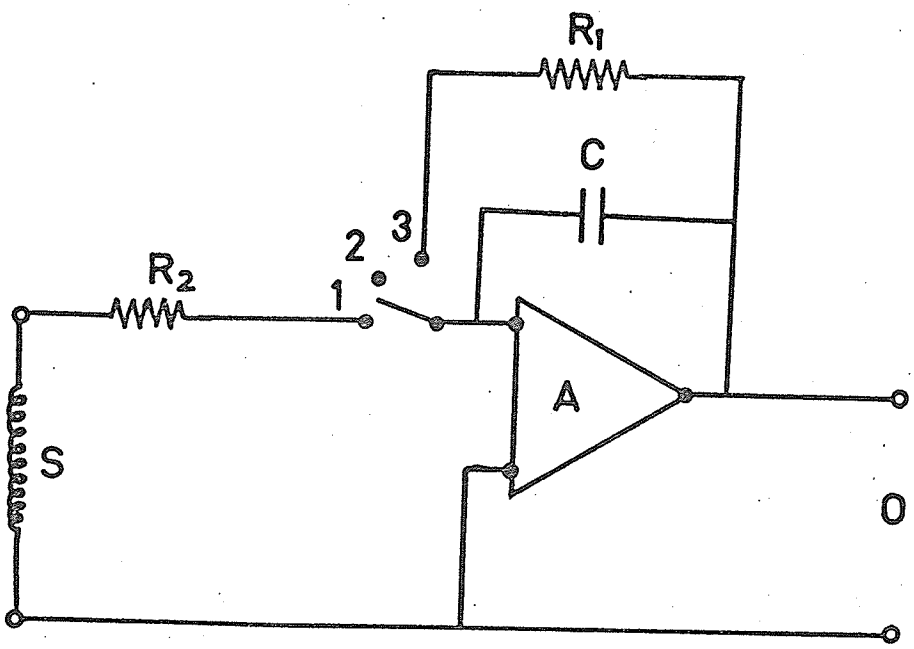

Fig. 3.1. Integrator Circuit.

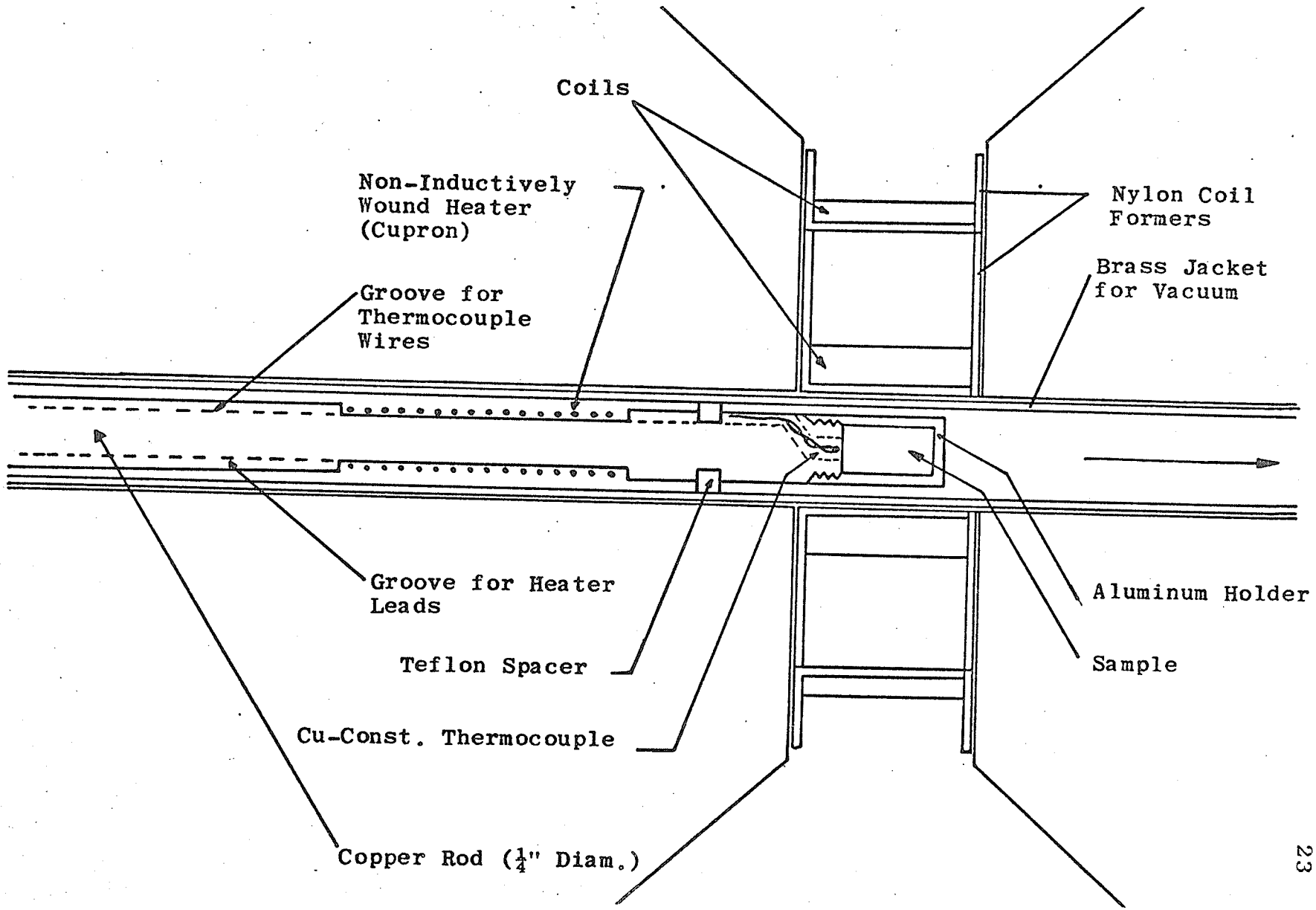

Fig. 3.2. Cold finger arrangement.

3.3 X-Ray Techniques

X-ray diffraction examination was carried out using a copper or iron target with appropriate filter

A single crystal rotation camera was used for most of the samples. This camera is useful for bulk samples and gives diffraction patterns similar to those of powders. Pictures were taken from samples which were mechanically polished, followed by chemical etching. Those samples were put in such positions, so that the collimated x-ray beam was striking them on one edge. The whole specimen was rotating about this edge with an amplitute of 16^{o}. Exposure times were about 4 - 5 hours, with an anode current of 20MA at 40kv for the copper tube.

In a few samples, the x-ray work was carried out by using the Debye-Scherrer method. For this purpose powder was required, which was provided by grinding some of the bulk specimen. The powder received the same heat treatment as the bulk sample and the results were satisfactory;giving an accurate value for the lattice parameters.

CHAPTER 4

OBSERVATIONS - MEASUREMENTS

4.1 General Review

In this section a brief review of the work done on all of the alloys is given. The basic idea is to see how the magnetic properties change for different systems and the possibility to relate this with changes in the crystal structure.

4.1.1 X-Ray Analysis

X-ray examination of the specimens after quenching and tempering at appropriate temperatures showed the existence of a phase transition of first kind from an disordered face centred cubic γ , to an ordered face centred tetragonal γ_1.

All the specimens quenched from 1,000° - 1,200° C contained a γ phase. At the first stage of ageing ordered lines appeared on the diffraction pattern, besides those of the cubic phase. On further ageing, the intensity of the disordered lines decreased while that of the γ_1 phase increased and after several hours of ageing only γ_1-phase lines could be seen on the pattern.

The transformation from cubic phase to tetragonal does not occur in the $FePt_{.6}Ni_{.4}$ alloy in which an

ordered cubic phase of the type $AuCu_3$ is formed while tempering.

The calculated lattice parameters are tabulated on Table 4.1. a_o refers to the cubic phase.

Table 4.1

Lattice Parameters of $FePt_{1-x}Ni_x$ Alloys

X	Heat Treatment	a_o (Å)	a (Å)	c (Å)	$\frac{c}{a}$
.2	Quenched from 1,280°C and aged for 2023 hrs. at 485°C.	3.770	3.823	3,690	.965
.3	Quenched from 1,100°C and aged for 100 min. at 700°C.	3.751	3.834	3.663	.955
.4	Quenched from 1,100°C.	3.730	---	---	---

4.1.2 Density

Knowing the atomic composition and the dimensions of the unit cell we can easily find the density of the alloys which is plotted against composition on diagram 4.2.

4.1.3 Optimum Magnetic Properties

The optimum magnetic properties of these alloys were developed after the appropriate heat treatment shown in Table 4.3.

According to these data $FePt_{.8}Ni_{.2}$ and $FePt_{.7}Ni_{.3}$ show good permanent magnetic properties while $FePt_{.6}Ni_{.4}$ shows very little magnetic hardening.

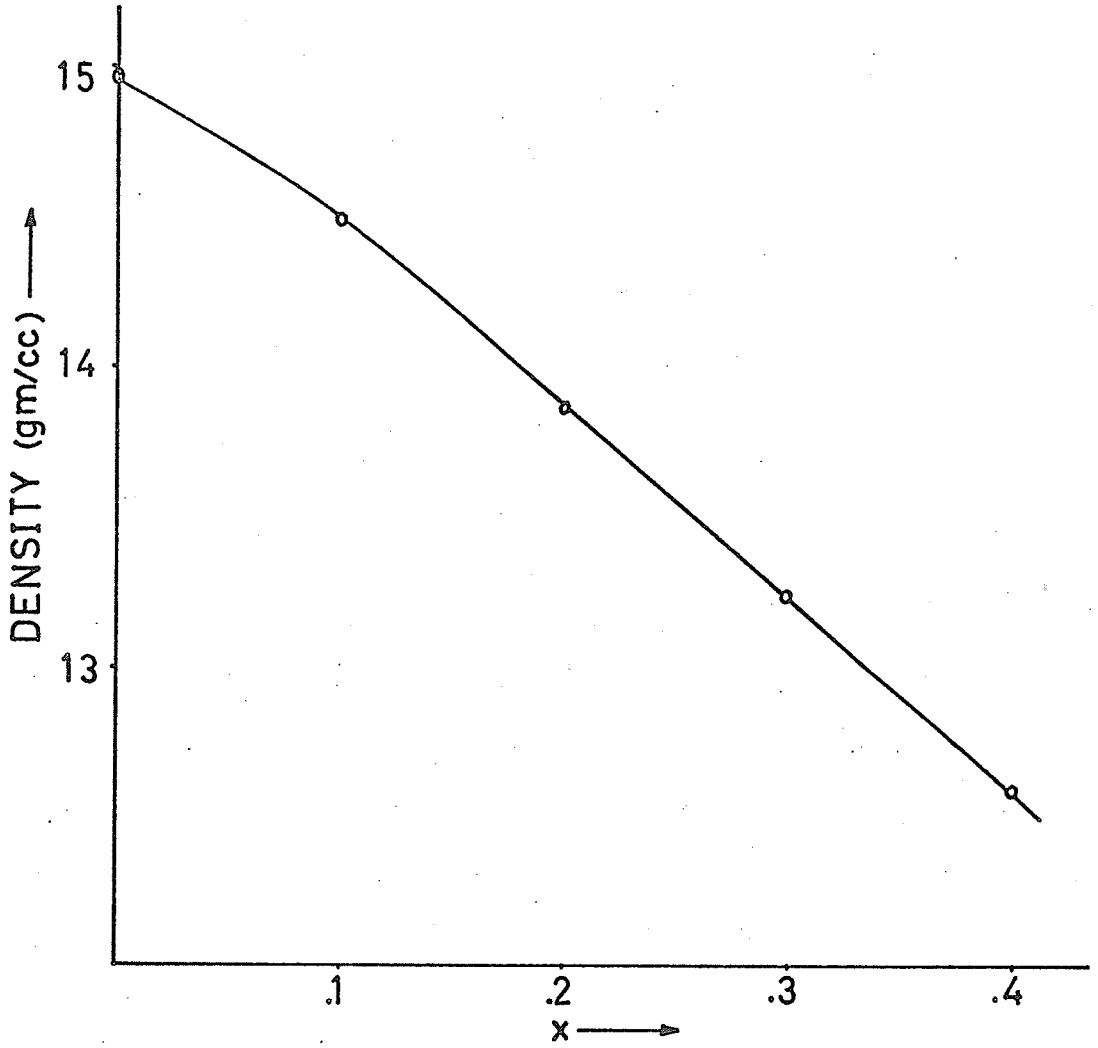

Fig. 4.2. The density as a function of composition.

Table 4.3

Optimum Magnetic Properties of $Pt_{1-x}Ni_xFe$

X	Ms(emu/gm.) Cubic Phase	Heat Treatment	Hc(Oe)	H_R(Oe)	Ms(emu/gm.)	M_R(emu/gm.)
.2	73.20	Quenched from 1,280°C aged for 105 hrs. at 485°C	2292	2660	61.8	32.6
.3	80.60	Quenched from 1,100°C aged for 35 hrs. at 650°C	1762	2100	70.1	34.8
.4	87.10	Quenched from 1,100°C aged for 169 hrs. at 650°C	370	558	87.2	14.4

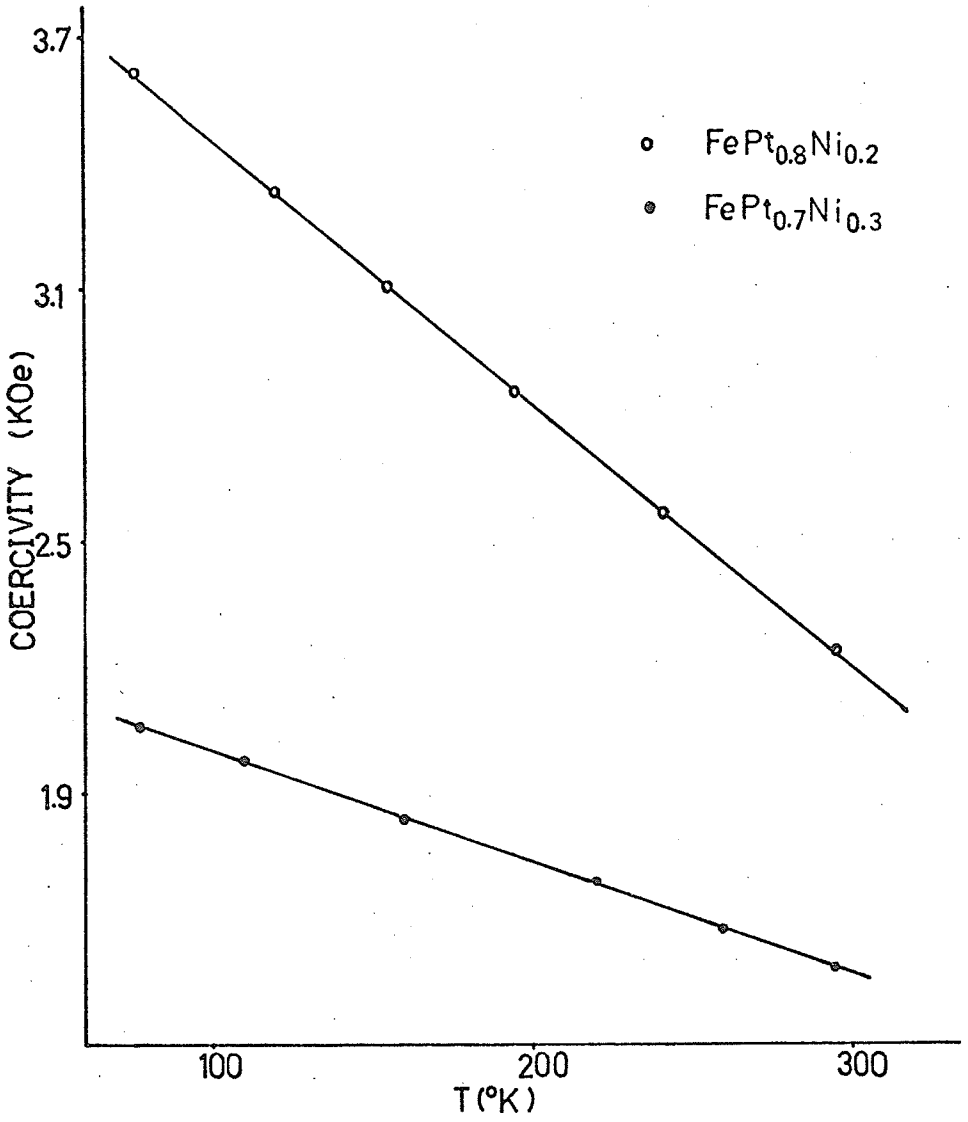

Fig. 4.4. Coercivity vs temperature.

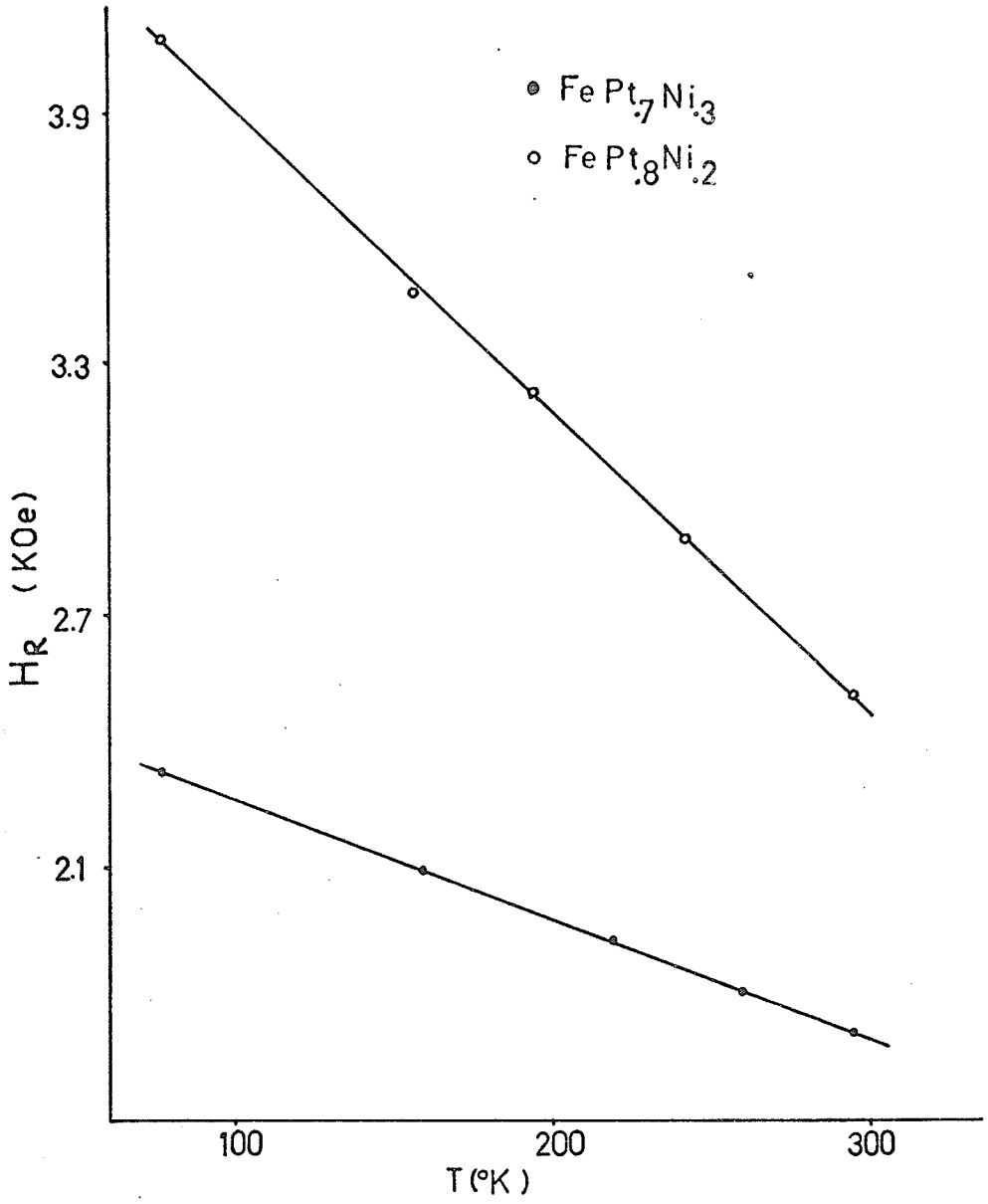

Fig. 4.5. Variation of remanence coercivity with temperature

4.1.4 Variation of Coercivity and Remanence Coercivity with Temperature

From experimental observations the coercive force Hc and remanence coercivity depend strongly on the temperature and they increase by a reasonable amount on cooling them to liquid nitrogen temperatures. The results are plotted on diagrams 4.4, 4.5. $FePt_{.8}Ni_{.2}$ was annealed for 67.5 hours at 485°C and $FePt_{.7}Ni_{.3}$ was annealed for 40.5 hours at 650°C. It is obvious from these figures that these functions depend linearly on the temperature.

4.1.5 $FePt_{.8}Ni_{.2}$ Alloy

The complete cycle of $FePt_{.8}Ni_{.2}$ is included in Table 4.6 which shows the variation of Hc and M_R at different aging times at 485 °C.

Table 4.6

Ageing Time (Hrs.)	Hc (Oe)	M_R (emu/gm.)
0	426	16.1
1.3	730	19.9
4	1,216	26.6
9	1,462	29.2
25	1,947	32.5
56	2,235	32.3
105	2,292	31.5
273	2,254	25.7
442	1,955	21.9
780	270	7.6

4.2 $FePt_{.7}Ni_{.3}$ Alloy

For more detailed work the $FePt_{.7}Ni_{.3}$ alloy was chosen because it has a relatively low transition temperature compared with $FePt_{.8}Ni_{.2}$ and because the magnetic properties of the two alloys are very similar.

4.2.1 Variation of Lattice Parameters with Ageing Temperature and Ageing Time

The lattice parameters of this alloy were investigated for various annealing times at different temperatures. The transformation from the disordered cubic to an ordered tetragonal doesn't occur above 750°C so that it suggests that its transition temperature lies within this range.

By using Cu $K\alpha$ radiation the lattice parameters were measured very accurately from high angle lines corresponding to 024, 332 reflection. From Tables 4.7, 4.8 we can easily see that the values of 'a' change slightly for different ageing times and more drastically at different ageing temperatures. At a given ageing temperature and for different ageing times the $\frac{c}{a}$ ratios for the structure and superstructure lines are the same, within an experimental error of $\pm$ .002.

The process is very slow at 600°C. The value of $\frac{c}{a}$ at the early stages of tempering differs from those at the subsequent ageing times. Particularly there is a reduction in $\frac{c}{a}$ by further tempering which

suggests that the degree of long range ordering is increasing.

At 650°C and 700° the process is rather fast and the values of $\frac{c}{a}$ are constant through all the ageing times. This indicates that the alloy orders quickly to the equilibrium degree of order.

The peculiar thing is that the degree of long range ordering is lower at 650°C than at 700°C whereas it would be expected to drop slightly for higher temperatures. This would suggest that the process here is not a simple ordering mechanism. The composition of this alloy is very close to the phase boundary of the ordered tetragonal and ordered cubic structure where the two ordered phases might coexist.

Table 4.7

Variation of Lattice Parameters With Ageing Time, Ageing Temperature 650°C

Ageing Time (hrs.)	c(Å)	a(Å)	$\frac{c}{a}$
.25	3.683	3.818	.965
4.00	3.678	3.808	.966
40.5	3.675	3.803	.966
Very long time	3.680	3.801	.968

(Estimated error in 'a' & 'c' = 0.001 Å)

Table 4.8

Variation of Lattice Parameters With Ageing Temperature

T (^{o}C)	Ageing Time (hrs.)	a^{o}_{A}	c^{o}_{A}	$\frac{c}{a}$
600	15.5	--	--	.967
	182	3.856	3.654	.948
650	4	3.808	3.678	.966
700	1.7	3.834	3.663	.955
	199	3.833	3.666	.956

4.2.2 Magnetization Curves

By quenching the specimen in water, after annealing it for several minutes at 1,000^{o}C, a disordered cubic structure was obtained. This phase is magnetically soft and it saturates at very low fields (Fig. 4.9). By further ageing at a certain temperature the saturation magnetization drops and remains fairly constant after a very long ageing time. This is thought to be associated with a tetragonal phase which is much harder than the cubic one (Fig. 4.10). Its magnetization saturates at very high fields which weren't available at this time. An attempt was made to find this saturation magnetization by plotting M vs $\frac{1}{H}$ and extrapolating it to infinite applied fields. The saturation magnetization

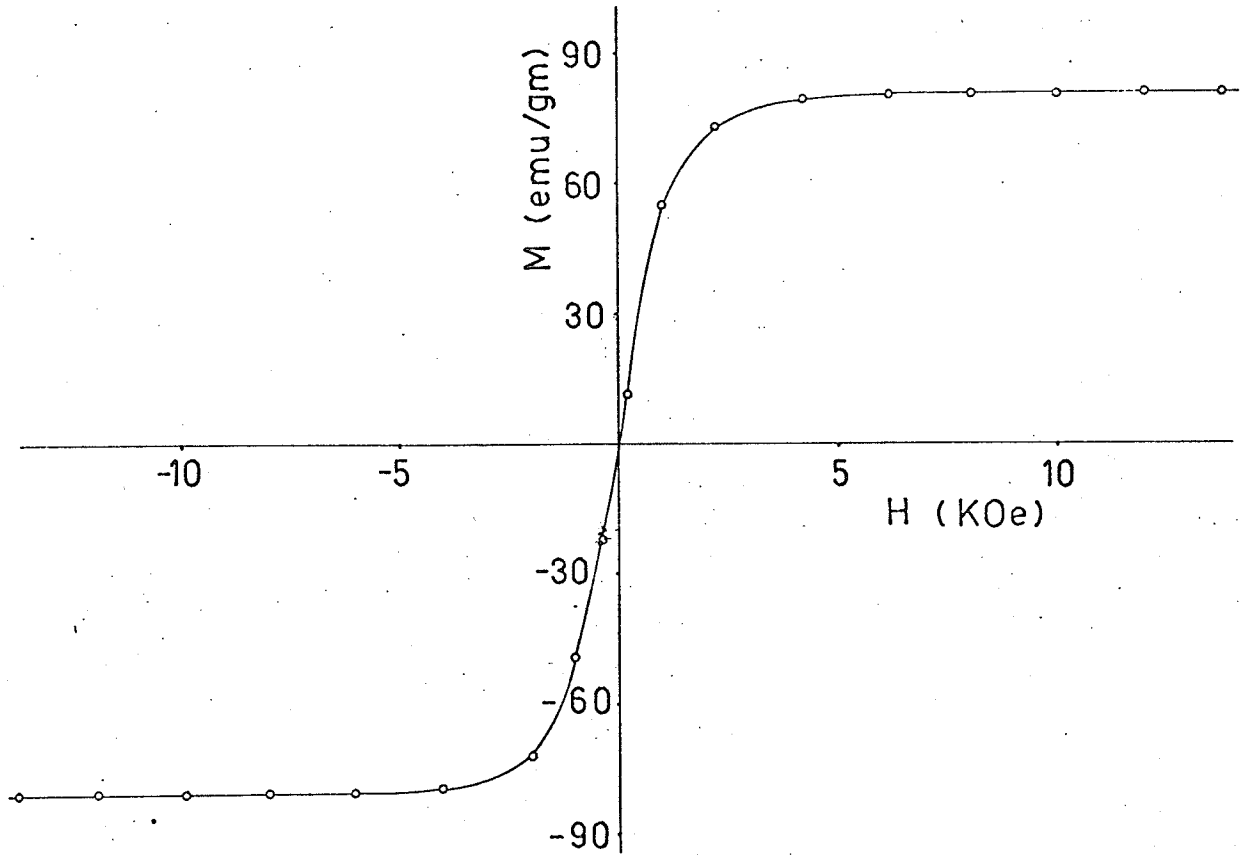

Fig. 4.9. Demagnetization curve for the cubic phase.

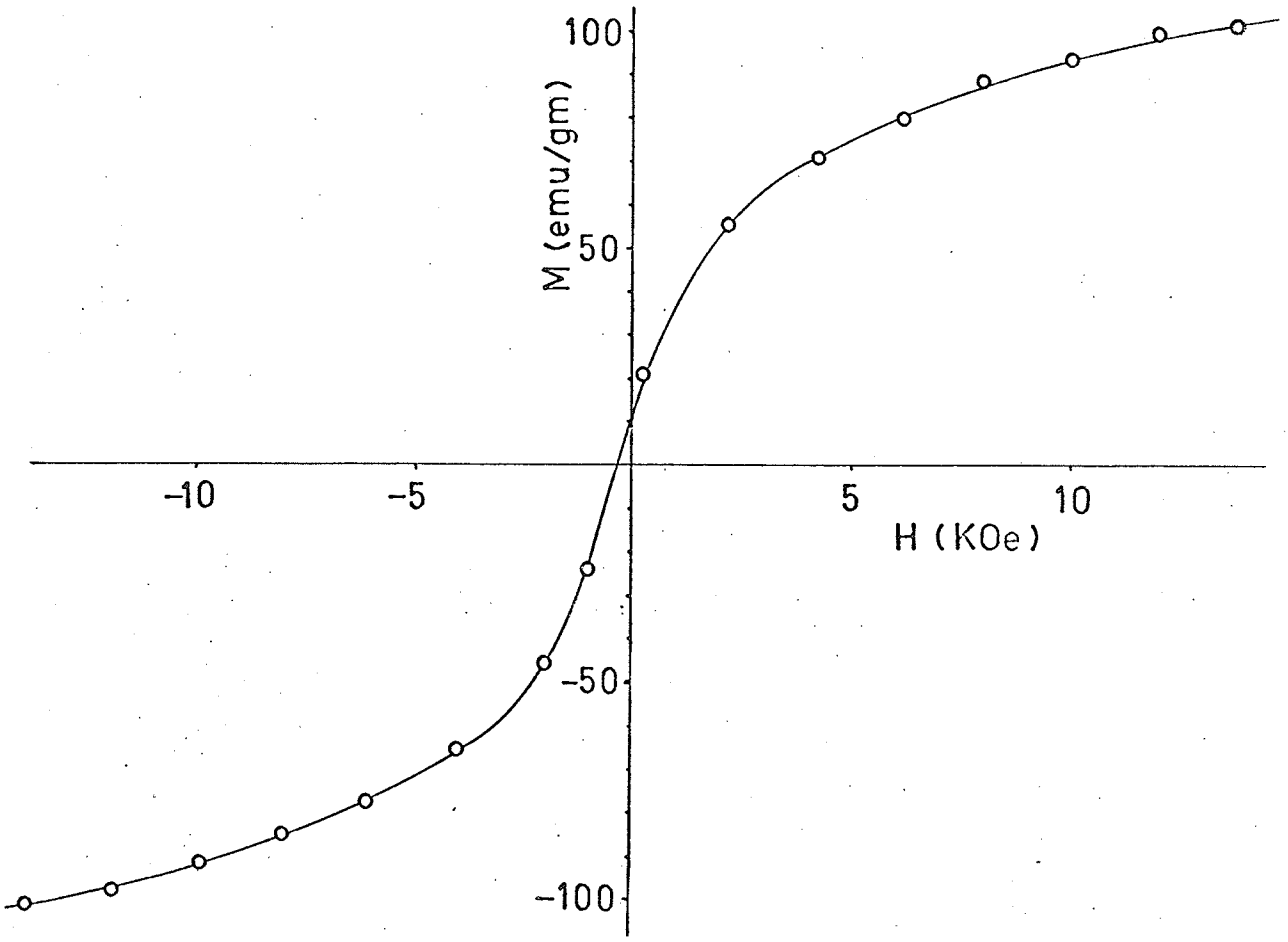

Fig. 4.10. Demagnetization curve for the tetragonal phase.

for both the phases are given in the following table.

	Cubic	Tetragonal
$Ms(\frac{emu}{gm})$	80.6	65.0

4.2.3 The Crystalline Anisotropy Constants

It is generally observed that magnetically hard materials possess a very high anisotropy energy. This crystalline anisotropy energy could be expressed in a series of trigonometric function. In a cubic crystal it must have cubic symmetry as it is given by[21]

$$W_k = k_1(a_1^2a_2^2 + a_2^2a_3^2 + a_1^2a_3^2) + k_2(a_1^2a_2^2a_3^2)$$

where k_1, k_2 are the anisotropy constants and a_1, a_2, a_3 the direction cosines between the direction of the magnetization and the cube edges. The anisotropy constants k_1, k_2 depend on the material used and their sign and magnitude determines the easy direction of the magnetization.

An attempt was made to find the order of the magnitude of the anisotropy constant k_1 by using the law of approach to saturation for polycrystalline specimens[22] (Gaus 1932, Becker-Doring 1939). According to this law

$$M_s - M = \frac{8k_1^2}{105M_sH^2} \qquad (1)$$

where M_s is expressed in $\frac{emu}{cc}$ and k_1 in $\frac{ergs}{cc}$. This law was modified by Neel[23] (1948) who took into account the interaction between the randomly oriented grains within the crystal. According to that

$$M_s - M = \frac{4k_1^2}{105M_s H^2} \qquad (2)$$

So by plotting Ms - M versus $\frac{1}{H^2}$ a straight line is obtained (Fig. 4.11). The slope of this line gives us the anisotropy constant k_1. By equation (1) it is found that $k_1 = -2.6 \times 10^6 \frac{ergs}{cc}$

and by equation (2) $k_1 = -3.6 \times 10^6 \frac{ergs}{cc}$

For the tetragonal phase the easy direction lies in the coaxis and the anisotropy energy is given by

$W_k = k_1' \sin^2\theta + k_2' \sin^4\theta$ where θ is the angle between the magnetization vector and the easy axis.

The magnitude of the anisotropy constant was roughly estimated by using U. W. Lee and J. E. L. Bishop method[24]. According to this

$$j = \frac{M}{M_s}, \quad h = \frac{HM_s}{k^I} = f\left(\frac{M}{M_s}\right)$$

Using our data we found a set of j's values and for each one the corresponding h, which were tabulated on certain tables. Then a plot of h against H should give us a straight line from the slope of which we can estimate the anisotropy constant k'. This is done in Fig. 4.12 and gives $k' \simeq 1 \times 10^7$ ergs/cc.

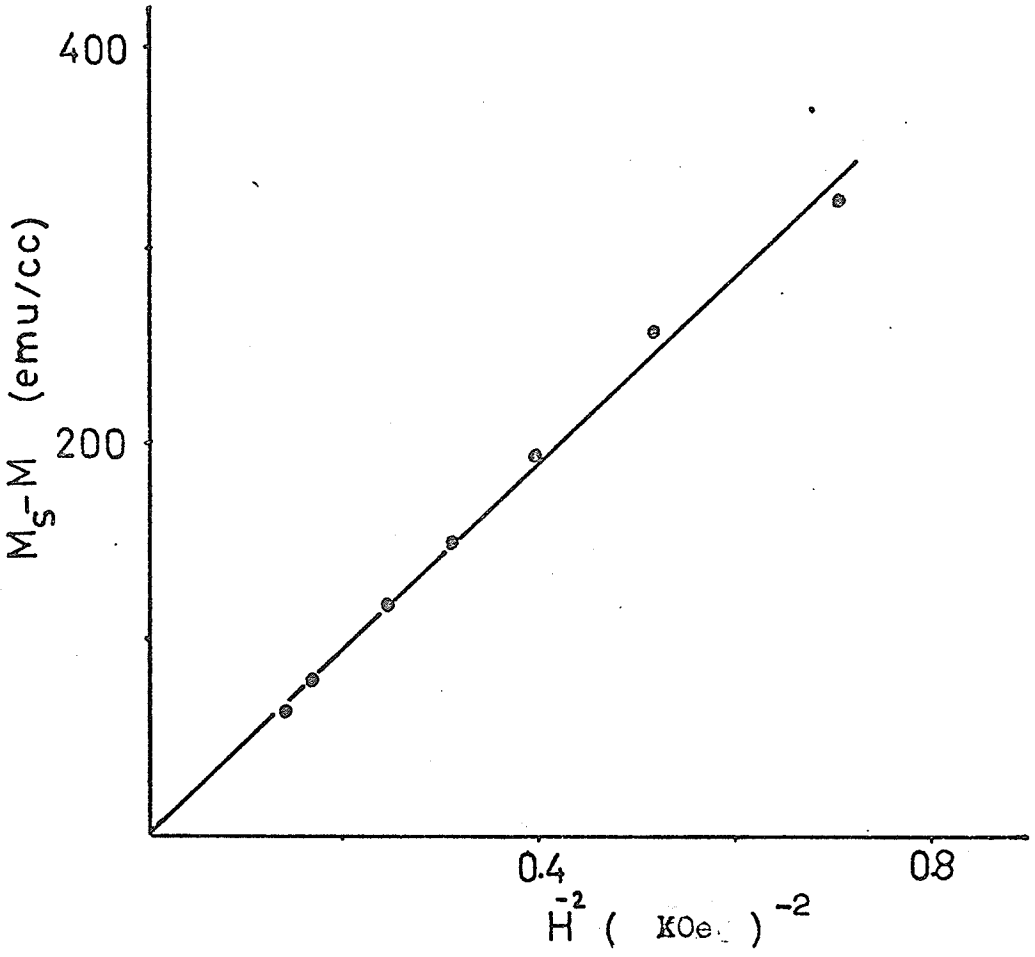

Fig. 4.11. Determination of k_1 for cubic phases from law of approach to saturation.

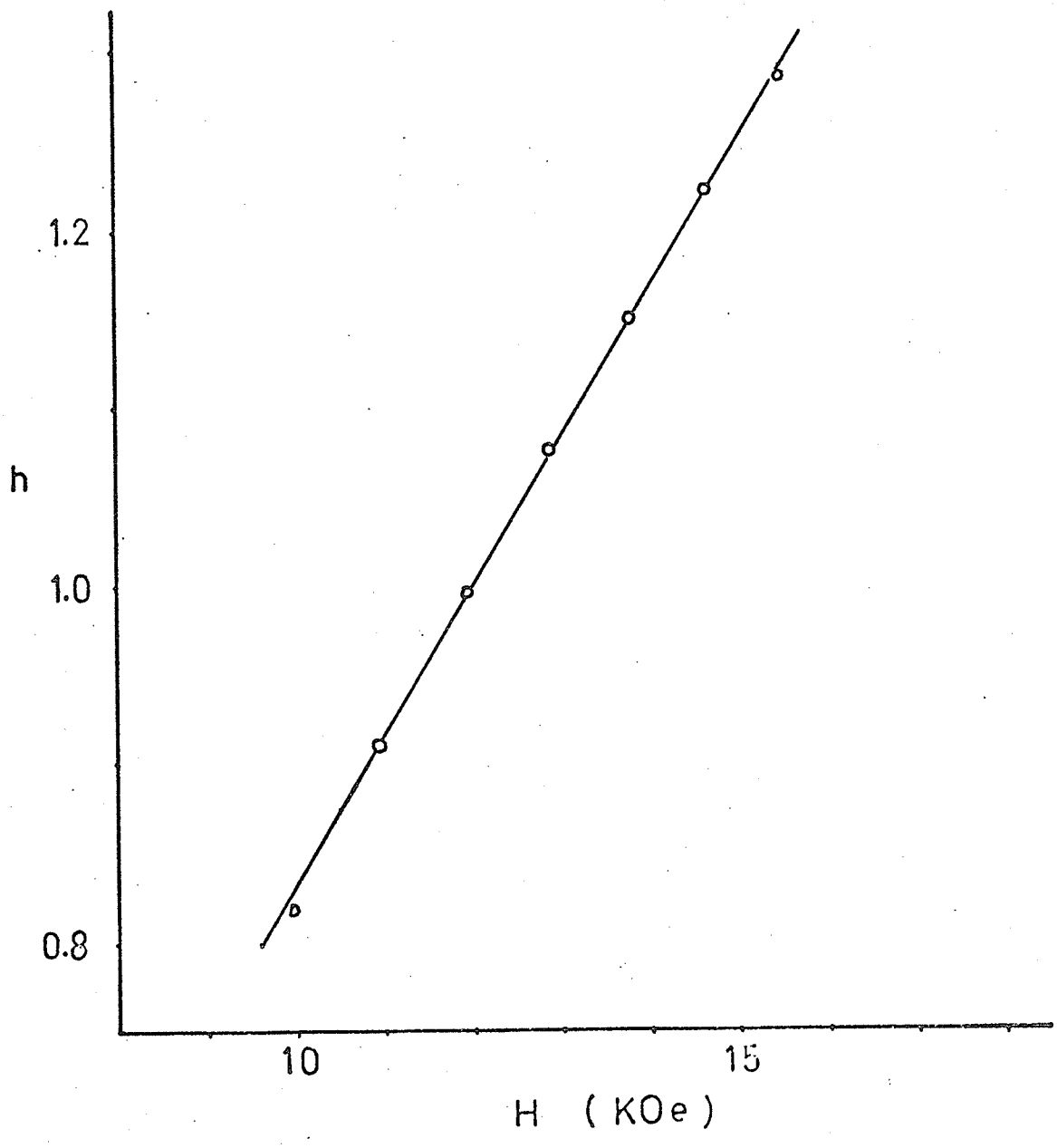

Fig. 4.12. Determination of k' for tetragonal phase.

4.2.4 Domain Wall Energy

In order to see how the domain wall energy varies for the tetragonal and cubic phase, we used the previously described (Stewart 1948) crude approximation which gives for the wall energy

$$\gamma = a\pi(2E|k|)^{\frac{1}{2}}$$

and for the domain wall width δ

$$\delta = a\pi\left(\frac{E}{2|k|}\right)^{\frac{1}{2}}$$

The exchange energy can be calculated by using the Weiss model

$$E = \frac{kTcM_s}{2\mu_B}$$

where K is the Boltzman constant, Tc is the Curie temperature, M_s is the saturation magnetization in emu/cc and μ_B the Bohr magneton.

We plotted our data in the above equations, using $a = 2.65\text{Å}$ and $T_c = 600^{\circ}K$. Knowing also that, in the case of cubic phase, the energy needed to rotate the magnetization from (111) direction to (110) is $W(111) - W(110) = \frac{k_1}{3}$, we substituted K with $\frac{k_1}{3}$. The obtained results are tabulated in the following table.

	E (ergs/cc)	γ (ergs/cm^2)	δ (Å)
Cubic	4.76×10^9	14.5	227
Tetragonal	3.84×10^9	23.1	115

4.2.5 Variation of Magnetic Properties with Ageing Time

The magnetic properties of this alloy were investigated for several ageing times. In Figures 4.13, 4.14, 4.15 the coercivity, the remanent magnetization and the remanence were plotted against lnt. Looking at these diagrams we can easily see that these quantities rise to a maximum and after they decrease, as the ageing time increases. It should be noted here, that the sample in the cubic phase has a negligible amount of coercivity, while after long ageing time the coercivity comes to a constant value which is higher than the starting one.

For a certain ageing temperature the ageing times for the maximum of coercivity and remanence are similar but the peak for the remanent magnetization curve comes at smaller times.

The peaks of these curves are shifted towards longer times as the temperature decreases. Figure 4.13 shows that, as the temperature decreases, the peak of the curves increases, but in Figure 4.14 there isn't too much change in the peaks for different annealing temperatures. The highest peak occurs at 650^{o}C and is

$$M_R = 39 \text{ emu/gm}.$$

4.2.6 Temperature Dependence of Coercivity and Remanence

The coercivity and remanence were measured in the range of 300^{o}K to 77^{o}K, for different ageing stages of the sample. The obtained results are plotted in Figures 4.16, 4.17, 4.18, 4.19. From these diagrams it may be seen that

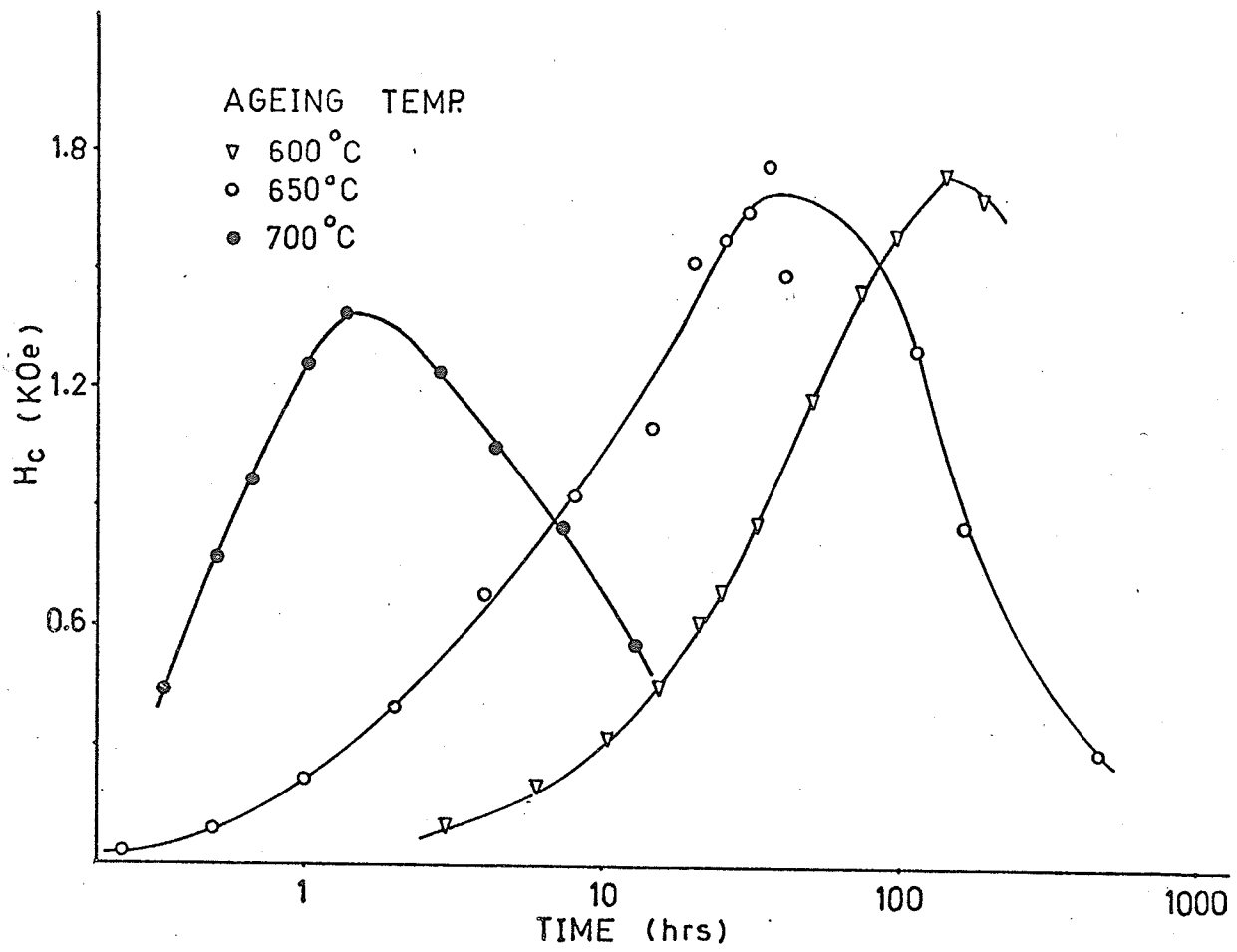

Fig. 4.13. The coercivity as a function of ageing time.

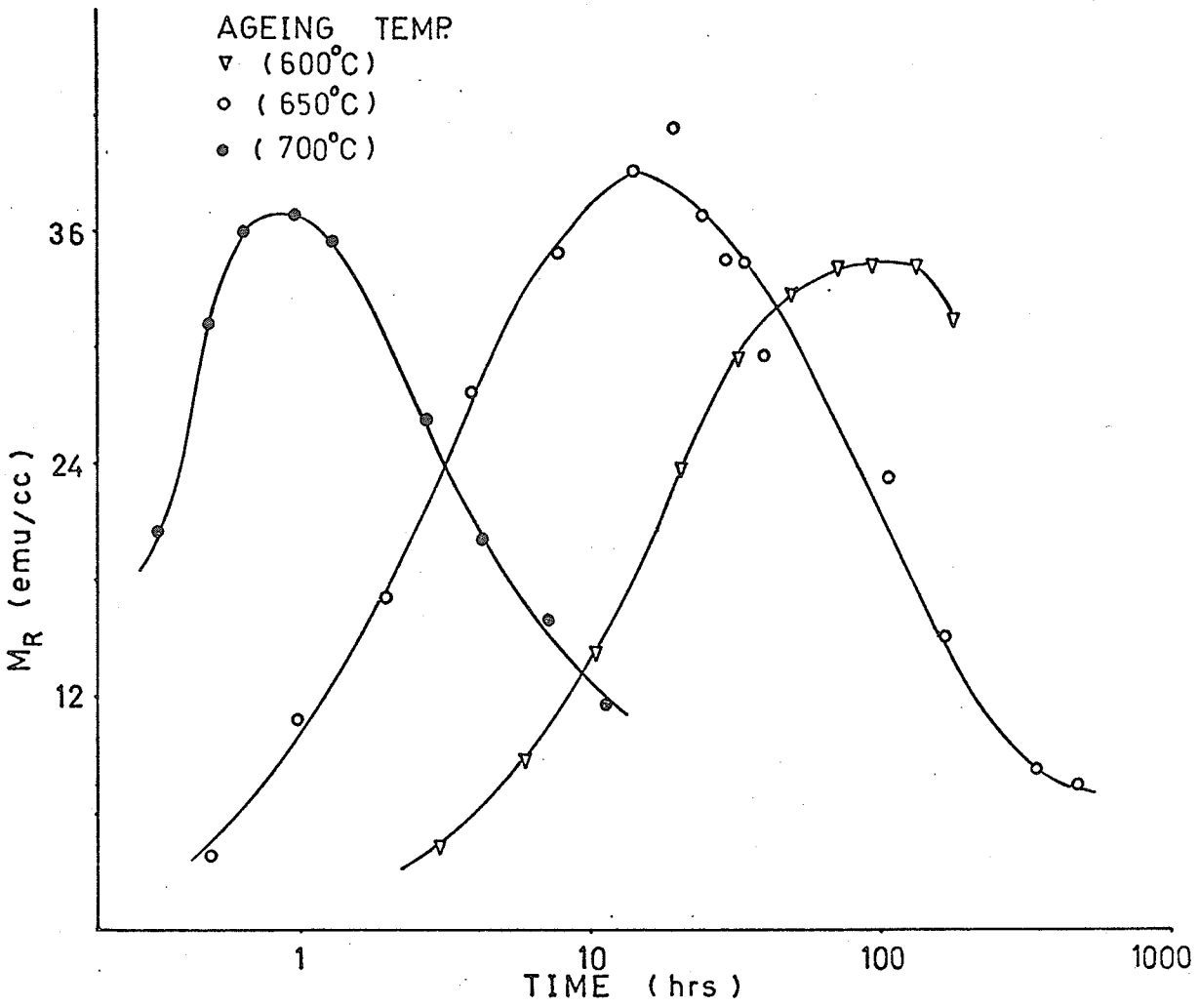

Fig. 4.14. The remanent magnetization as a function of ageing time.

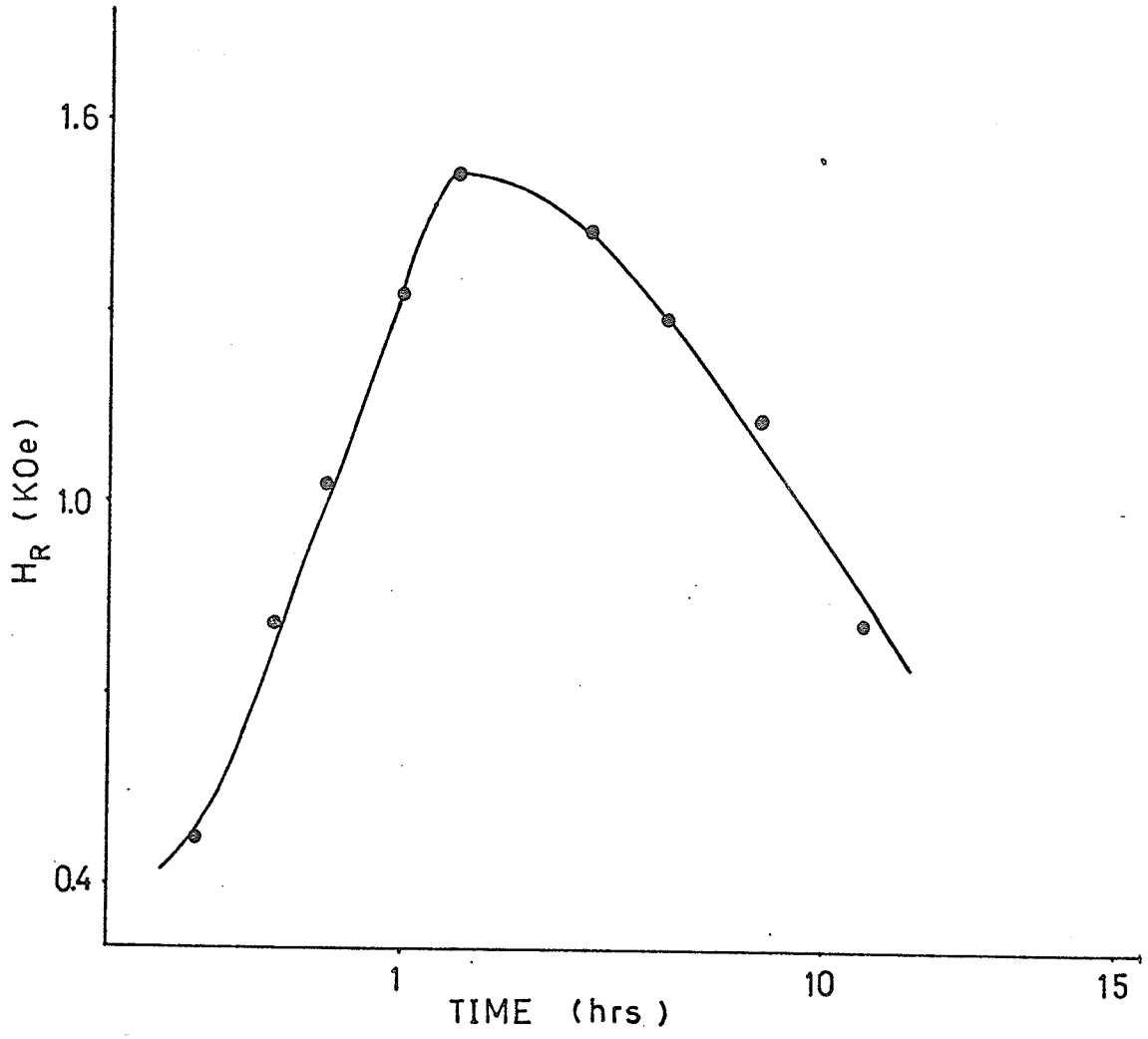

Fig. 4.15. The remanence coercivity as a function of ageing time. Ageing temperature 700°C.

the coercivity and remanence vary linearly with temperature. As the ageing time increases, the slope of these lines rises to a maximum value and after it decreases again to become almost zero after very long ageing time.

It is observed that for ageing at 700°C the rate of change of coercivity with temperature is higher than that of the remanence coercivity. The maximum slope of these curves is that for the H_R of the sample aged at 600°C.

From these figures we can find Hc(O) and $H_R(O)$, the coercivity and remanence coercivity at absolute zero, by extrapolating these lines to zero temperature. Also the values for the reduced slope, given by $\frac{Hc(O)}{(\frac{dHc}{dT})}$, can be calculated. The obtained results for $FePt_{.7}Ni_{.3}$ aged at 700°C, 650°C, 600°C near its optimum point are tabulated on Table 4.20.

4.2.7 Demagnetization and Remanence Curves for different Stages of the Sample

The demagnetization and remanence curves were investigated for several ageing stages of the sample. From Figure 4.21 it can easily be seen that the coercive force Hc and the remanence H_R differ slightly. Looking at Figures 4.22, 4.23, 4.24, 4.25 we can say that at the early stages of ageing the effect of the temperature on the magnetic parameter is stronger than that at the later stages.

4.3 Discussion of Results and Further Suggestions

We may summarize all of the observations we've already discussed in previous sections. We started from a stage, where the sample was all cubic, and it had a negligible coercivity. We estimated roughly its anisi-

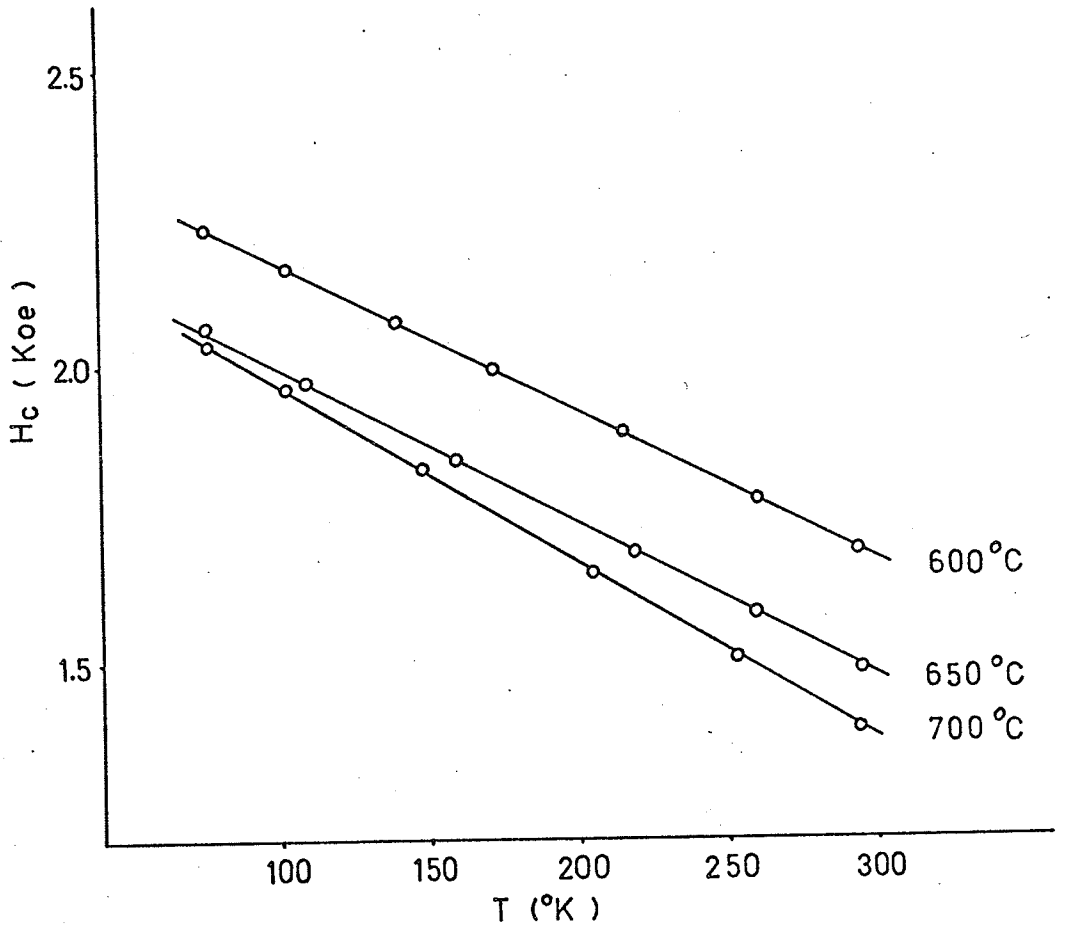

Fig. 4.16. Temperature dependence of coercivity. Sample aged at 3 different temperatures, noted on the figure.

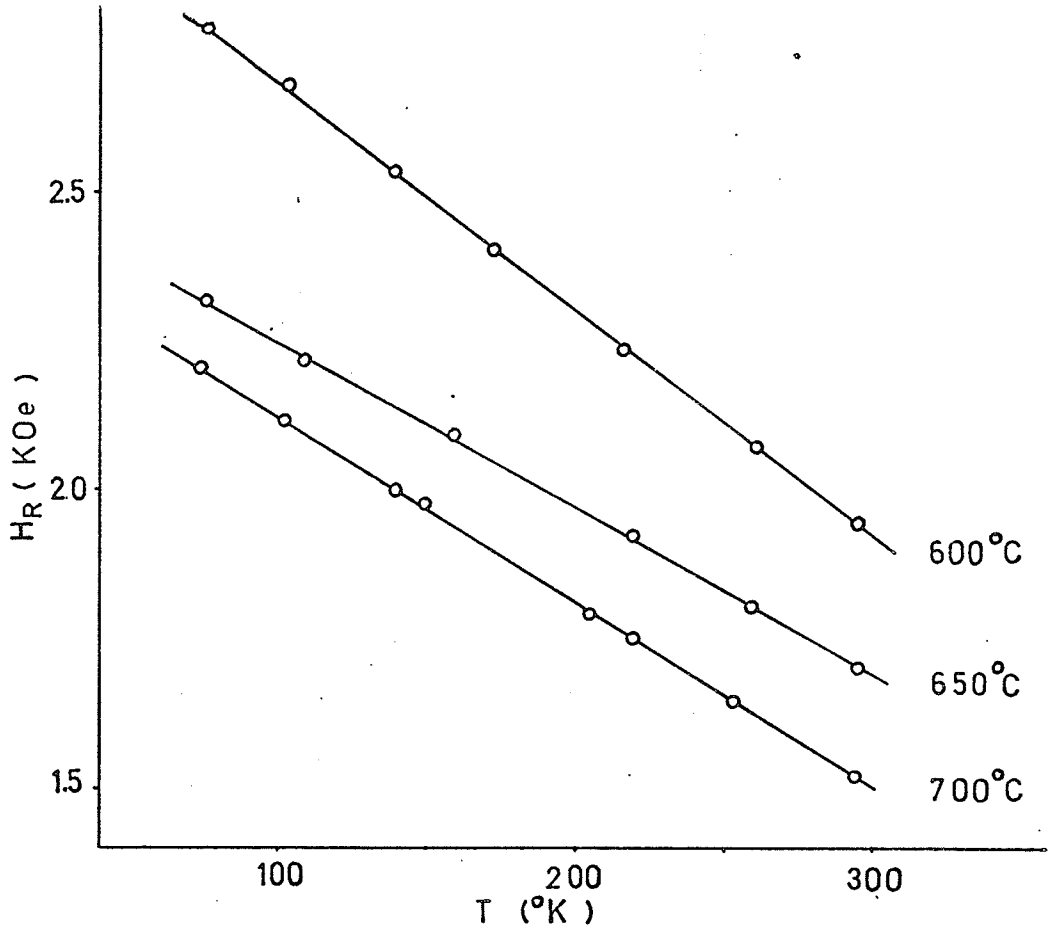

Fig. 4.17. Temperature dependence of remanence coercivity. Sample aged at three different temperatures, noted on the figure.

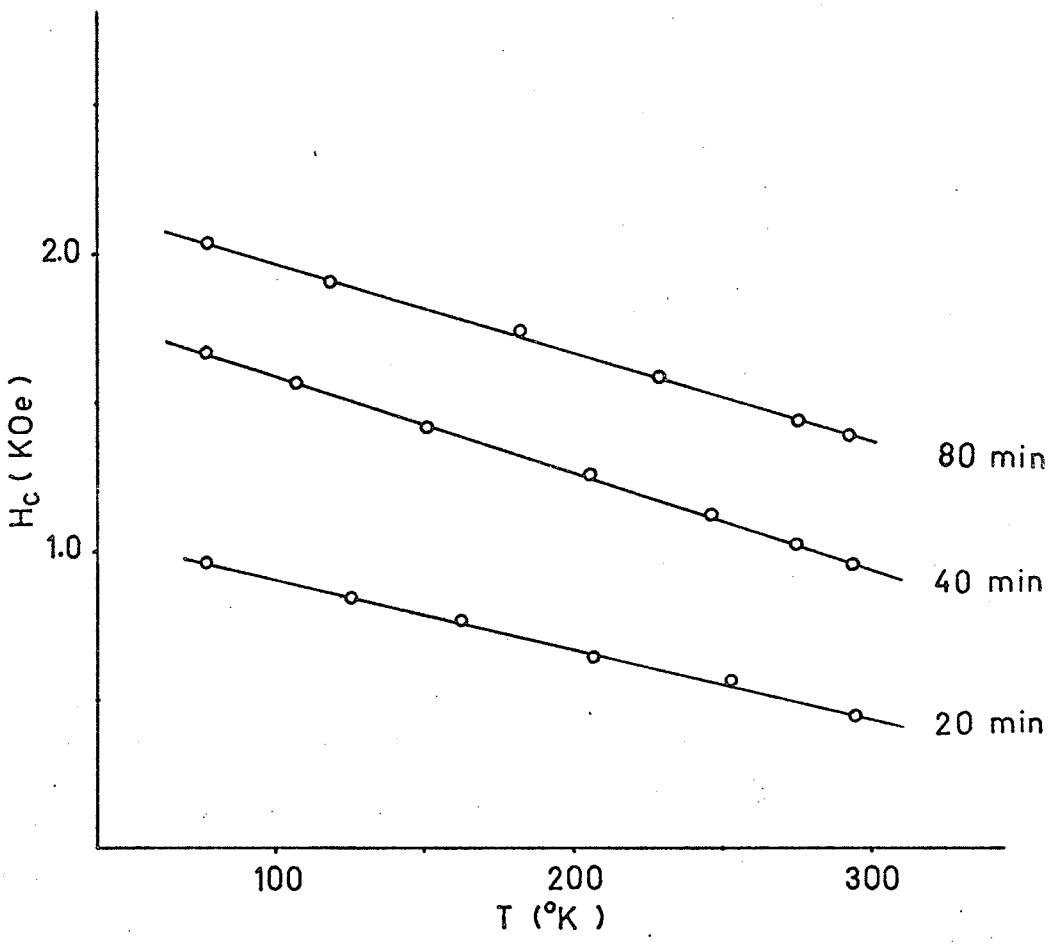

Fig. 4.18. Temperature dependence of coercivity. Sample was aged for 20, 40, and 80 min. at 700°C.

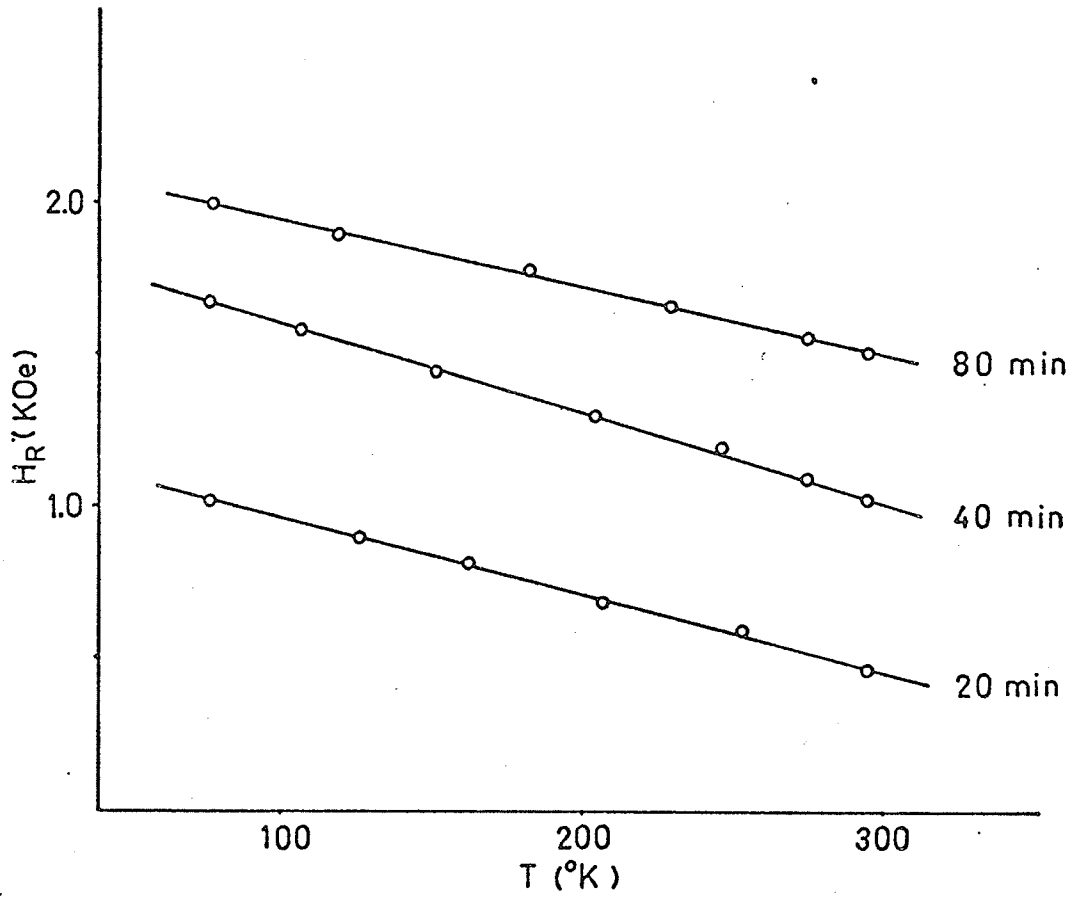

Fig. 4.19. Temperature dependence of remanence coercivity Sample was aged for 20, 40 and 80 min. at 700°C.

Table 4.20

Values of the reduced Slope $\frac{Hc(O)}{\frac{dH}{dT}}$ for three different ageing temperatures

Heat Treatment	$H_c(O)$ (Oe)	$\frac{Hc(O)}{\frac{dHc}{dT}}$ (°K)	$H_R(O)$ (Oe)	$\frac{H_R(O)}{\frac{dH_R}{dT}}$ (°K)
Aged at 600°C for 182 hrs.	2420	968	3070	819
Aged at 650°C for 40.5 hrs.	2250	918	2530	886
Aged at 700°C for 80 min.	2270	783	2430	778

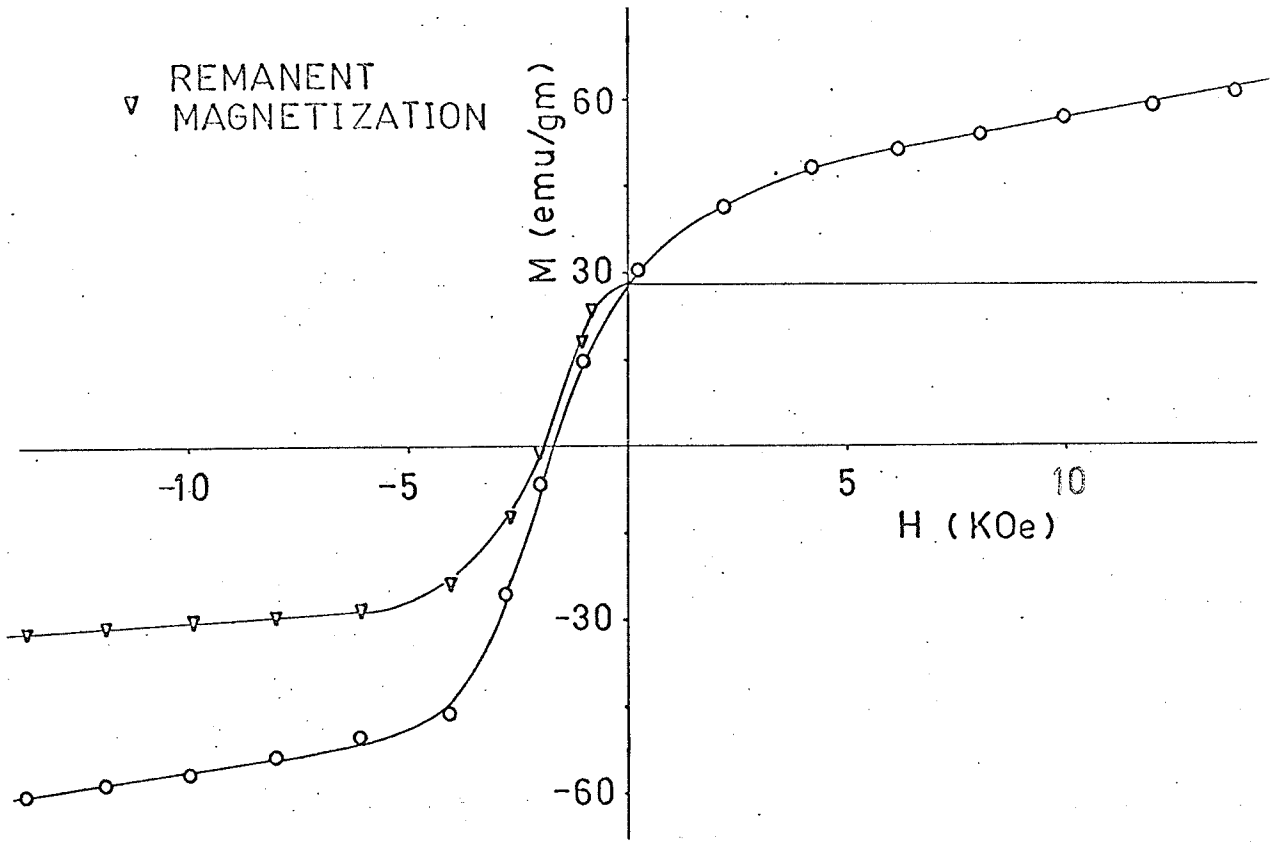

Fig. 4.21. Demagnetization and remanence curve for $FePt_{.7}Ni_{.3}$ aged at 600°C for 182 hrs.

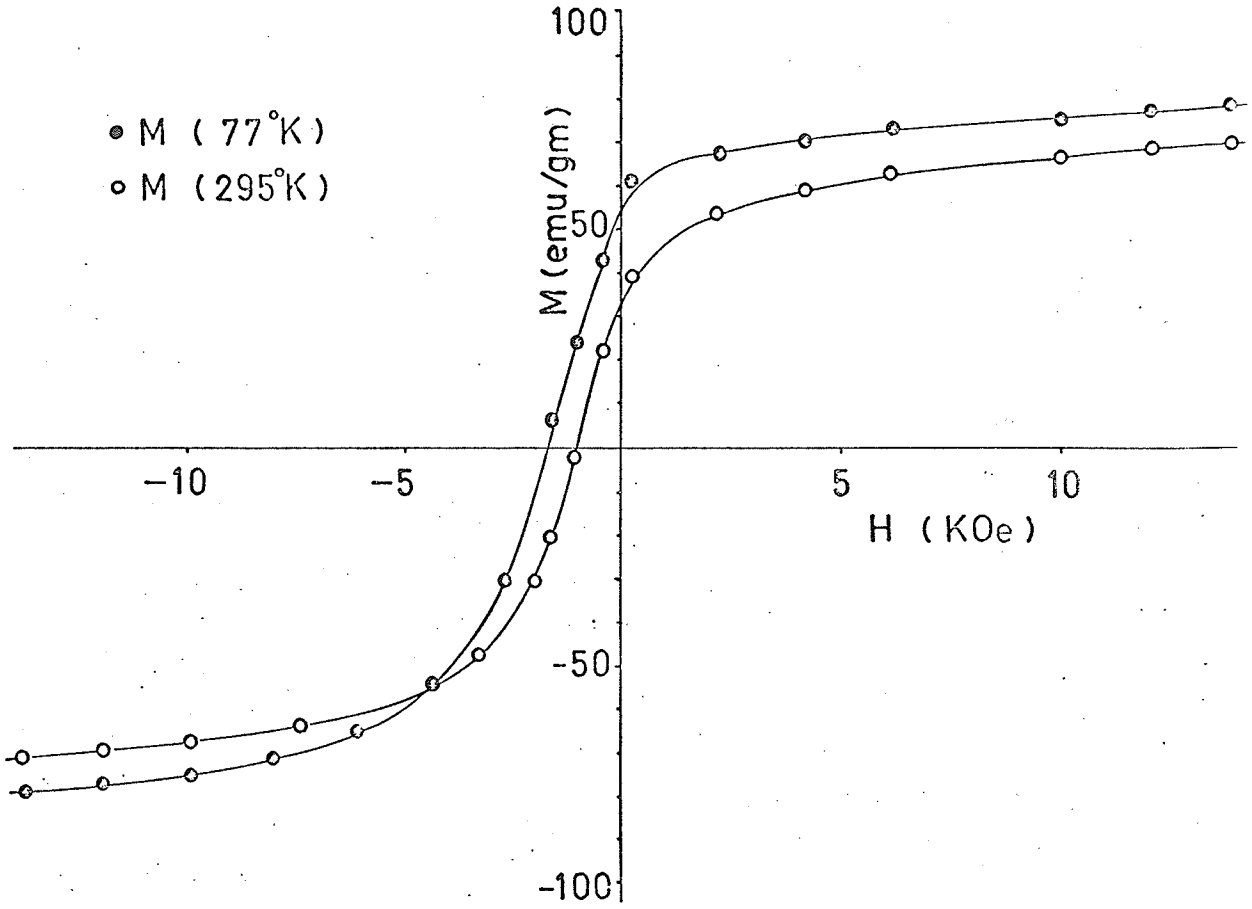

Fig. 4.22. Demagnetization curve for $FePt_{.7}Ni_{.3}$ aged for 40 min. at 700°C.

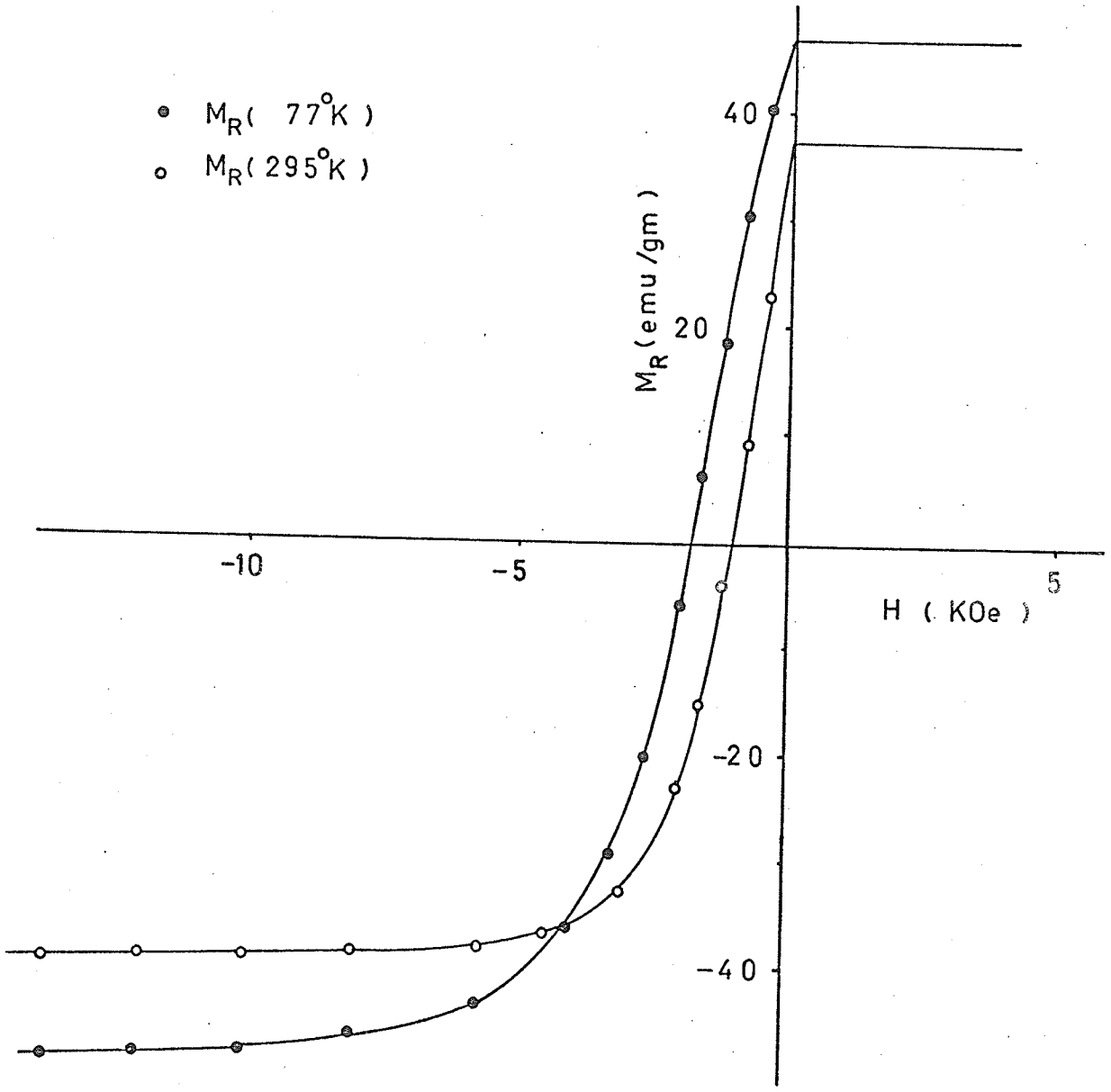

Fig. 4.23. Remanence curve for $FePt_{.7}Ni_{.3}$ aged for 40 min. at 700°C.

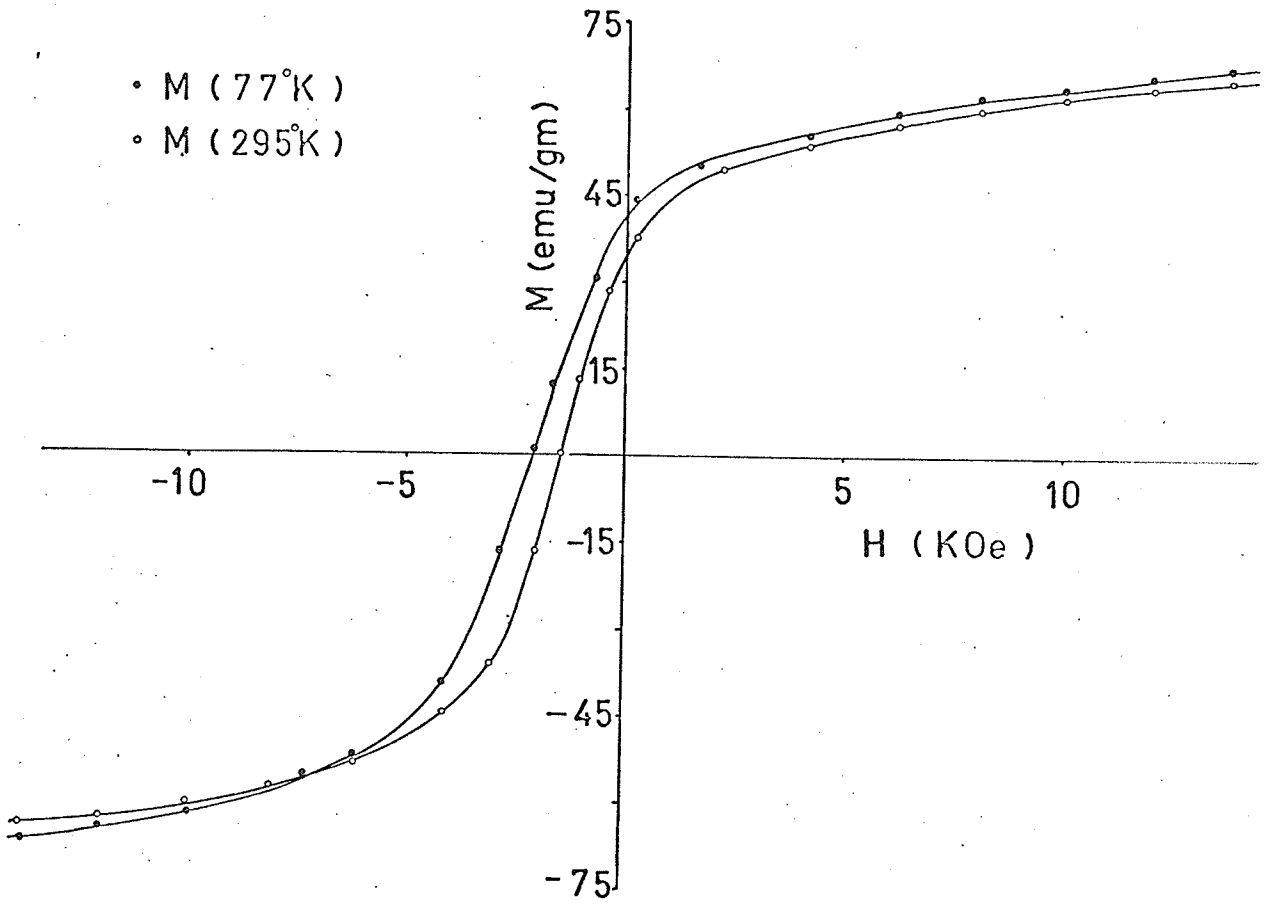

Fig. 4.24. Demagnetization curve for $FePt_{.7}Ni_{.3}$ aged for 80 min. at 700°C.

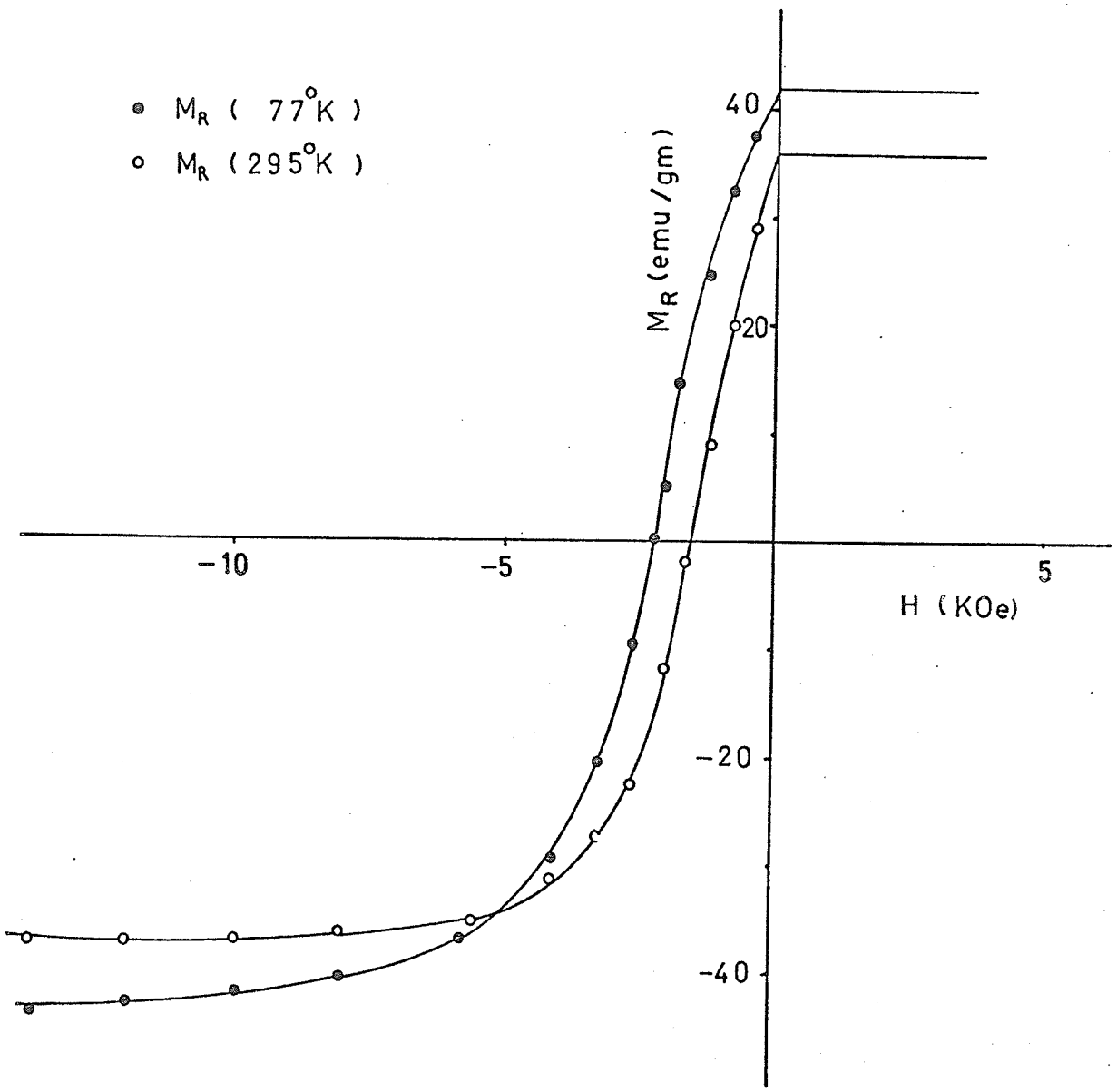

Fig. 4.25. Remanence curve for $FePt_{.7}Ni_{.3}$ aged for 80 min. at 700°C.

tropy constant and we found it fairly high $K_1 = 4 \times 10^6$ ergs/Oe. Regardless of the used ageing temperature, the tetragonal phase started appearing in the x-ray pictures, at the early stages of ageing as an indication of the cubic to tetragonal transformation. Even in this stage, where the two phases coexist, i.e., tetragonal particles in a cubic matrix, the measured coercivity was found to be fairly low. The transformation from cubic to tetragonal was completed after a short time and the tetragonal phase was the only one that appeared in the x-ray pictures. With this phase present, the coercivity increased with ageing time up to a maximum value, and after it started decreasing again to become almost constant for very long ageing times. At this stage the anisotropy constant was estimated to be of the order of $K_1 = 1 \times 10^7$ erg/Oe, which is very close to the value the anisotropy has for the cubic case. However, it should be noted also, that the difference in the wall energies of the tetragonal and cubic phase, is not very high.

From all we have seen, it seems that the mechanism for magnetic hardening in these alloys differs from that of CoPt.[25] It is suggested that for CoPt, the magnetic hardening could be explained by assuming a finely disperse mixture of ordered and disordered phases. According to this, small tetragonal particles of high anisotropy constant, present in a cubic matrix, could pin the domain

wall and give rise to the observed hardening. It is also found that for CoPt the anisotropy constant of the cubic phase is low compared with that of $FePt_{.7}Ni_{.3}$ and that the difference between the domain wall energies of the tetragonal and cubic phase is three times bigger than the difference in $FePt_{.7}Ni_{.3}$. However, according to the model of domain wall pinning by inhomogeneities a large and abrupt change of the wall energy with position is required, for high coercivities. For $FePt_{.7}Ni_{.3}$ this change in the domain wall energy can't be associated with the difference between the wall energy of the tetragonal and cubic phase because this difference is very low. On the other hand, as the x-ray pictures show, there isn't a mixture of two phases but only one single phase is present in the sample.

Having all of these observations in mind, we may suggest that in the early stages of annealing, the cubic phase transforms to a tetragonal matrix with small misoriented tetragonal islands embedded in it. As the annealing time increases, these islands tend to lign with the main matrix, so that their size decreases giving rise to the coercivity. By this process the coercivity comes to a maximum value corresponding to a size of these islands for which the pinning is most effective. By further annealing their size becomes so small that it is ineffective for wall pinning and finally they join the main matrix.

The simplest case to consider is a 180° domain wall with an inhomogeneity of cross sectional area a within it (Fig. 4.26). Assuming that the spins within the wall are normal to the page of the diagram and that the easy axis of the inhomogeneity is parallel to the spins, then there is no contribution to the wall energy from this area and the change in the domain wall energy from the whole pinned area A could be equal to

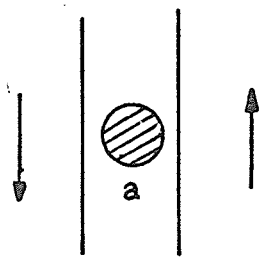

Fig. 4.26

$$A\Delta\gamma \simeq a\gamma_t = \frac{Ho}{\frac{dHc}{dT}}$$

From the values of table 4.20, we can easily see that the reduce slope remains fairly constant for annealing at different temperatures and different times. By averaging all of these values and substituting in the above equation we may estimate the cross sectional area of the inhomogeneity a which is found to be

$$a = 1.3 \times 10^{-13} cm^2$$

Following this model we may easily explain the linear dependence of coercivity and remanence on temperature.

However, the assumptions we made they are very crude. Further work needs to be done in order to test the above suggestions. For this purpose a single crystal of the specimen is necessary andit will provide us with enough information of the structural changes within the

sample. Extra spots should appear on the diffraction patterns, due to the various misorientations of the tetragonal islands from the main matrix. Such extra spots would confirm the hypothesis.

Electron microscopy and diffraction of thinned samples would allow observation of the structure of a single crystal area and its misorientations. The interaction of magnetic domain walls with the misoriented regions could be observed for the same area using Lorentz electron microscopy.

REFERENCES

1. P. Weiss (1907). Journal of Physics, 6, 667.

2. C. Kittel (1949). Reviews of Modern Physics, 21, 541.

3. W. F. Brown, Jr. (1940). Physical Review, 58, 736.

4. K. H. Stewart (1954). Ferromagnetic Domains (Cambridge University Press, p. 93).

5. R. Becker, W. Doring (1939). Springer, Berlin, Ferromagnetismus.

6. M. Kersten (1944). Grundlagen einer Theories der Ferromagnetischen Hysterese und der Koerzitivkraft, Hirzel, Leipzig.

7. L. Neel (1946). Ann Unive. Grenoble 22, 299.

8. Stoner-Wohlfarth (1948). Philosophical Transactions, 240, 599.

9. P. Gaunt (1972). Journal of Applied Physics, 43, 637.

10. R. A. McCurrie (1965). Ph.D. Thesis, University of Sheffield.

11. L. Graf, A. Kussman (1935). Phys. Z., 36, 544.

12. H. Lipson, D. Shoenberg, G. Stupart (1941). Journal of Institute and Metals, 67, 333.

13. A. Kussman, G. Ritteberg (1950). Z. Mellk 41, 470.

14. L. Weil (1948). J. Phys. Radium 9, 203.

15. G. Ivanova (1970). Fiz metal metalloved, 29, 175.

16. N. Vlasova, Z. Vintaykin (1968). Fiz. metal metalloved 27, 631.

17. S. Shimizu, E. Hashimoto (1971). Journal of the Japan Institute of Metals, 35, 902.

18. N. Vlasova, T. Sapozhkova (1970). Fiz. metal metalloved, 30, 980.

19. J. Pauleve, D. Dautreppe, J. Lauqier, L. Neel (1962). Compt. Rend, 254.

20. A. Ferro, G. Griffa (1971). Nuovocimento, 3, 269.

21. A. Morrish (1965). The Physical Principles of Magnetism, p. 313.

22. R. Gaus (1932). Ann. Physik, 15, 28.

23. L. Neel (1948). J. Phys. Radium, 9, 184.

24. E. W. Lee, J. E. L. Bishop (1966). Proceedings of Physical Society, 89, 661.

25. P. Gaunt (1966). Philosophical Magazine, 13, 579.